Bulletin of Earthquake Engineering (2019) 17:1285–1330
https://doi.org/10.1007/s10518-018-0501-y

ORIGINAL RESEARCH

Empirical drift-fragility functions and loss estimation for infills in reinforced concrete frames under seismic loading

Carlo Del Gaudio[1] · Maria Teresa De Risi[1] · Paolo Ricci[1] · Gerardo Mario Verderame[1]

Received: 5 December 2017 / Accepted: 12 October 2018 / Published online: 24 October 2018

Abstract
Earthquakes that have occurred in the last twenty years in the Mediterranean area have had significant economic and social impacts. Most of the economic losses of reinforced concrete (RC) frames was due to nonstructural component damage, particularly masonry infills and partitions. Therefore, the seismic behaviour of masonry infills should be reliably characterized. The main goals of this study for a more reliable loss estimation for infilled RC frames are: (i) the analysis of the inter-story drift ratio (IDR) capacity at given damage states (DSs) with the aim to define drift-based fragility functions and (ii) analyse direct losses due to infill damage following seismic events. First, a database of experimental tests performed on 1-bay, 1-story scaled RC frames infilled with clay bricks or concrete blocks is collected. Drift-based fragility curves are obtained, which depend on the infill brick materials and properties. Then, the drift capacity threshold at each DS is correlated to the in-plane response of the infill panel to directly quantify the relationship that exists among them. The influence of openings on drift capacities is also evaluated. Then, seismic losses related to infills are computed, providing expected monetary losses depending on the infill typology. The required reparation activities and their costs are also listed. The bearing of each activity and cost at each DS is explicitly evaluated. Additionally, loss functions that directly depend on IDR demand are provided, thus fusing together the damage analysis and loss analysis. Finally, a simplified formulation for loss functions is proposed for a simple, practice-oriented loss calculation.

Keywords RC buildings · Masonry infills · Brick typology · Experimental data · Damage states · Fragility curves · Loss functions

Maria Teresa De Risi—beneficiary of an AXA Research Fund postdoctoral grant.

✉ Maria Teresa De Risi
mariateresa.derisi@unina.it

Extended author information available on the last page of the article

1 Background and objectives

Earthquakes that have occurred in the last twenty years in the Mediterranean area have had significant economic and social impacts. For example, in Italy, after the 6th April 2009 earthquake affecting the Abruzzi region, over 10,000 million euros were allocated for emergencies and reconstruction. Much of the funds for reinforced concrete (RC) frames were due to damage to nonstructural components, namely, infills and partitions (Dolce and Goretti 2015; Del Gaudio et al. 2016a, b). Therefore, seismic performance assessments of infilled RC frames must also consider infills to properly estimate the expected seismic losses. This aspect is also more important due to the diffusion of infilled RC frames as a constructive solution, especially in the Mediterranean area. To this end, the seismic behaviour of masonry infills should be reliably characterized through the definitions of the following: (i) the infill drift capacities in different damage states (DSs), (ii) the required repair activities following an earthquake and (iii) the relative costs of these activities.

Recently, this issue was addressed by valuable studies (commented on below), focused on (i) the definition of inter-story drift ratio (IDR) thresholds and their uncertainties corresponding to given physical damage levels on infill partitions and, in a few cases, on (ii) the seismic loss estimation due to infills. Some researchers proposed the definitions of different DSs through the observation of the extent and severity of cracking patterns on the panels or about the failure of brick units. Some others also related such damage levels to the attainment of the infilled frame's peak strength or the attainment of given strength decay thresholds. Typically, three or four DSs have been defined in the literature, corresponding to (i) the onset of cracking and first detachment between the infill panel and surrounding RC frame, (ii) the widening of the previous damage pattern, (iii) the crushing and spalling of several brick units and (iv) the partial/total collapse of the panel.

The European Macroseismic Scale (EMS-98) (Grünthal 1998) first proposed three DSs specifically for infill panels in RC frames as a function of a qualitative description of damage (fine cracks, large cracks, and collapse). *Agibilità e Danno nell'Emergenza Sismica* (AeDES) (usability and damage in post-earthquake emergency) survey forms (Baggio et al. 2007) also define three DSs reporting a more accurate and detailed damage description with a quantitative indication of crack widening for each DS.

Later, Colangelo (2013) defined four DSs, strictly relating infill IDR capacity to the infill panel's in-plane response. In such a way, DS1 is related to the first noticeable reduction in stiffness and to the onset of cracking in bricks; DS2 is related to a moderate damage pattern before attaining the maximum strength; DS3 is related to an extensive damage pattern and to the failure of a few brick units; and DS4 is related to infill panel failure. Colangelo (2013), based on pseudodynamic tests on RC frames infilled with hollow clay bricks, proposed the estimation of probabilistic parameters of the drift capacity at these DSs within a fuzzy-random approach to the damage assessment.

More recently, Cardone and Perrone (2015) reported a definition of DSs similar to AeDES survey forms, adding a fourth DS, and reporting further indications about the width of diagonal cracks and the extension of the panel area affected by cracks or the possible failure of some brick units. In some cases, Cardone and Perrone (2015) arbitrarily assumed a relationship between the attainment of the ith DS (with $i = 1,\ldots,4$) and the characteristic points of the backbone, particularly the peak load point. Based on approximately fifty tests of infills (with clay bricks or concrete blocks, with and without openings, and with different frame typologies), Cardone and Perrone (2015) conducted drift-based fragility functions with no distinction in terms of brick material due to the limited number of

data. For the same reason, the fragility function distinction due to the presence of openings has not been performed based on collected tests but through assumptions from the literature (Dolšek and Fajfar 2008). Loss functions have finally been proposed in a FEMA P-58 (2012b) approach for a specific hollow clay infill typology.

Based on a similar experimental database and DSs definition, in Sassun et al. (2016), drift-based and equivalent diagonal strut-strain-based fragility curves were proposed for infills with solid clay bricks and clay units with vertical holes, concluding that, whenever possible, the seismic performance assessment of an infill should consider the masonry infill typology, especially in the case of a larger amount of data. Repair cost estimates for infills in Italy were also computed by using costing manuals and comparing them with cost estimates obtained through consultation with some Italian building contractors.

Finally, Chiozzi and Miranda (2017) introduced a damage classification based on three DSs, basically different from the abovementioned DSs due to the quantification of crack widths. No information about the extension of damage or the percentage of damaged units is provided in this case, making this definition less objective. Chiozzi and Miranda (2017) considered a large amount of experimental data related to different frame typologies (RC or steel frames) or brick typologies and configurations (with or without openings). These researchers analysed the influence of some parameters (mechanical properties, brick typology or the eventual presence of openings) on drift capacity, always classifying all the data in some (nonhomogeneous) subsets of data for a single parameter at a time. No loss analysis is provided in this work.

1.1 Research significance

In the present study, the damage analysis and loss analysis are investigated for infills with *clay bricks or concrete blocks*—typical of Italian and Mediterranean building stock—in RC frames. The main goals of the study for a more reliable loss estimation are (i) the analysis of the drift capacity at given DSs aiming at the definition of drift-based fragility functions and (ii) the analysis of direct loss due to damage to infills after seismic events.

Therefore, first, a wide database of experimental tests on scaled 1-bay, 1-story RC frames infilled with clay bricks or concrete blocks—some of which was performed by the authors—is collected and presented. In particular, based on 105 tests characterized by the description of the damage evolution under increasing drift demand, the drift capacity at given performance levels is quantified. Then, empirical cumulative distribution functions are evaluated for four different DSs, and lognormal fragility functions are used to fit such data. The collected database has been divided into homogeneous data subsets, thus deriving drift-based fragility curves, which explicitly depend on brick materials and infill main properties. The drift capacity thresholds at different DSs have also been correlated to the peak load point of the in-plane response of the infill panels where possible, to directly and explicitly quantify the relationship that exists among them. The influence of openings on drift capacities is also considered through the analysis of experimental campaigns, which tested both infilled frames with openings and the related frames infilled with a solid panel, used as reference, being the same all the other variables.

Finally, seismic losses related to infills are computed, providing expected monetary loss, also in this case depending on the infill typology. All the required repair activities and their costs are listed. Their percentage weight at each DS is explicitly evaluated as a function of drift demand. Loss functions directly depending on IDR demand are finally provided, thus

fusing together damage analysis and loss analysis, also in a simplified, closed (fitted) form for a simple, practice-oriented loss calculation.

2 Collected experimental tests

The first step of the present research is the collection of a comprehensive database of tests on infilled RC frames. More than 300 experimental tests performed and presented in the literature over the last four decades have been analysed and divided into homogeneous subsets depending on the infill and frame typology. Tests performed on 1-bay, 1-story RC frames (199 overall) and in particular, tests completely characterized by the authors in terms of geometrical and mechanical properties with clay or concrete bricks (136 tests) have been considered. Starting from such a database, only tests completely characterized by the description of damage evolution to the infill panel have been selected (105 tests), given the main goals of this work. In summary, the main features of the data analysed in this work are graphically reported in Fig. 1.

The majority of the collected tests (75%) were performed on solid panels, namely, panels without openings. The remaining part (25%) was performed on infill panels with door or window openings. Generally, collected infills were realized with clay bricks (Cl-B)—approximately 72% of tests—which is the most common brick typology worldwide. Less tests (28% of tests) dealt with concrete blocks (C-B). Tests with clay brick infills have been further classified into (i) solid bricks (S-Cl-B) and (ii) hollow bricks (H-Cl-B), depending on the presence or absence of holes, whereas infills with concrete blocks have been classified into normal concrete blocks (NC-B) and autoclaved aerated concrete blocks (AAC-B).

Overall, the collected database includes 105 tests, thus representing a wide collection of data specifically referring to RC infilled frames. Such a database should be considered as an extension of those already presented in the literature, such as the extensive database collected in Chiozzi and Miranda (2017), characterized by 81 tests on RC frames with clay or concrete infill panels, or the databases collected in Cardone and Perrone (2015) and Sassun et al. (2016). Both are characterized by almost 40 tests related to the typology investigated herein.

Tables 1 and 2 report the main geometrical properties related to tests without and with openings, respectively. H_w and L_w represent the height and length of the infill panel, respectively; t_w is the infill wall thickness, and the void percentage characterizes the percentage of holes, if any. Note that approximately 70% of the specimens are characterized

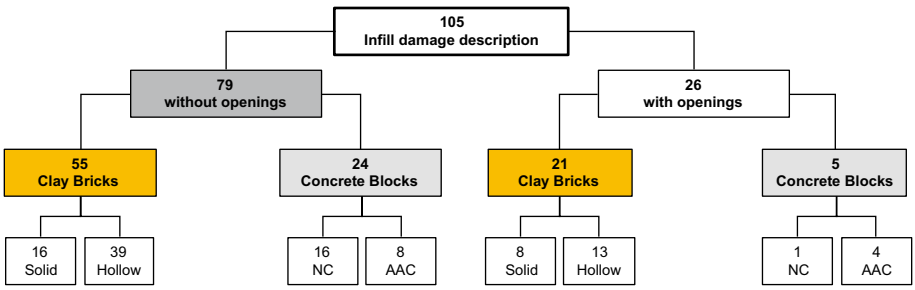

Fig. 1 Experimental tests from the literature adopted in this study (*NC* normal concrete blocks, *AAC* aerated autoclaved concrete blocks)

Table 1 Collected database of infilled RC frames without openings

#	References	Label	Scale	Holes*	Bt	Void (%)	t_w (mm)	H_w (m)	L_w (m)	FM**
1	Angel et al. (1994)	2a	1:2	–	S-Cl-B	0	48	1.63	2.74	–
2		3a	1:2	–		0	48	1.63	2.74	–
3		6a	1:2	–		0	98	1.63	2.74	–
4		7a	1:2	–		0	98	1.63	2.74	–
5		8a	1:2	–		0	187	1.63	2.74	–
6	Chiou and Hwang (2015)	B39L	1:1	–		0	200	2.64	6.80	SS
7		B39T	1:1	–		0	200	2.64	6.80	SS
8	Gazic and Sigmund (2016)	O3_cpm	1:2	–		0	120	1.30	1.85	SS
9		O4_cpm	1:2	–		0	120	1.30	1.85	SS
10		O1_cpm	1:2	–		0	120	1.30	1.85	SS
11		O1_cvm	1:2	–		0	120	1.30	1.85	SS
12		O2_cpm	1:2	–		0	120	1.30	1.85	SS
13	Khoshnoud and Marsono (2016)	F1	1:4	–		0	55	0.65	0.90	SS
14	Kyriakides and Billington (2008)	1	1:5	–		0	95	0.56	0.99	SS
15	Mansouri et al. (2014)	S	1:2	–		0	106	1.30	2.10	SS
16	Stavridis (2009)	CU1	2:3	–		0	95	1.86	3.38	SS
17	Baran and Sevil (2010)	SP9	1:3	V	H-Cl-B	52	70	0.75	1.30	CC
18	Bergami and Nuti (2015)	Ft1	1:2	V		50	120	1.30	2.30	CC + SS
19	Cavaleri and Di Trapani (2014)	s1b2	1:2	V		30	150	1.60	1.60	DC

Table 1 (continued)

#	References	Label	Scale	Holes*	Bt	Void (%)	t_w (mm)	H_w (m)	L_w (m)	FM**
20	Colangelo (2005)	C1	1:2	V		53	120	1.30	1.70	DC
21		C2	1:2	V		53	120	1.30	1.70	DC
22		L1	1:2	V		53	120	1.30	2.30	CC + SS
23		L2	1:2	V		53	120	1.30	2.30	CC + SS
24		N1	1:2	H		54	160	1.30	2.30	CC
25		N2	1:2	H		54	160	1.30	2.30	CC
26	Gazic and Sigmund (2016)	O3_bpm	1:2	V		50	120	1.30	1.75	DC
27		O4_bpm	1:2	V		50	120	1.28	1.75	DC
28		O1_bpm	1:2	V		50	120	1.30	1.85	CC
29		O1_bvm	1:2	V		50	120	1.30	1.85	–
30		O1_bpm*	1:2	V		50	120	1.30	1.85	CC
31	Guidi et al. (2013)	URM_U	1:1	V		50	300	2.65	4.15	–
32	Haider (1995)	A1	1:1	V		23	89	2.07	2.01	DK
33		B1	1:1	V		23	89	2.07	1.91	DK
34		D2	1:1	V		23	89	2.07	1.45	DK
35	Kakaletsis and Karayannis (2008)	S	1:3	H		36	60	0.80	1.20	DC
36	Misir et al. (2016)	IWF	4:5	V		50	235	2.00	3.20	CC
37	Morandi et al. (2014)	TA2	1:1	V		50	350	2.95	4.22	CC
38	Sigmund and Penava (2012)	2/III	1:2	V		55	120	1.30	1.80	SS
39	Waly (2010)	2	1:2	H		34	110	1.25	1.75	DC
40	Zarnic and Tomazevic (1984)	M2	1:2	V		30	150	1.50	2.08	DK

Table 1 (continued)

#	References	Label	Scale	Holes*	Bt	Void (%)	t_w (mm)	H_w (m)	L_w (m)	FM **
41	Zovkic et al. (2013)	Model 4	1:2	V	H-Cl-B	40	120	1.30	1.80	CC + SS
42		Model 8	1:2	V		50	120	1.30	1.80	DK + SS
43	Calvi and Bolognini (2001)	6	1:1	H		60	115	2.75	4.20	–
44	Colangelo (2005)	V11	1:2	H		64	80 + 80	1.30	2.30	CC
45		V21	1:2	H		64	80 + 80	1.30	2.30	CC
46		V22	1:2	H		64	80 + 80	1.30	2.30	CC
47	DIST Unina†	GI-120	1:2	H		66	120	1.35	2.10	–
48	Misir et al. (2016)	SWF	4:5	H		69	220	2.00	3.20	–
49	Pereira et al. (2011)	Ref_Wall	2:3	H		60	150	1.70	3.50	–
50	Ricci et al. (2017)	IP + OOP_L	2:3	H		60	80	1.83	2.35	–
51		IP + OOP_M	2:3	H		60	80	1.83	2.35	–
52		IP + OOP_H	2:3	H		60	80	1.83	2.35	–
53	Akhound et al. (2015)	MIF-I-2LNC	1:2	H		60	140	1.64	2.42	CC
54	Verderame et al. (2016)	GI-80	1:2	H		60	80	1.35	2.10	CC
55		SI-80	1:2	H		60	80	1.35	2.10	DC
56	Angel et al. (1994)	4a	1:2	–	NC-B	0	92	1.63	2.74	–
57		5a	1:2	–		0	143	1.63	2.74	–
58	Centeno et al. (2008)	1	1:2	–		–	100	1.85	1.83	SS
59	Crisafulli (1997)	Unit 1	3:4	–		0	90	2.00	2.52	SS
60	Mehrabi et al. (1996)	4	1:2	V		48	92	1.42	2.13	SS

Table 1 (continued)

#	References	Label	Scale	Holes*	Bt	Void (%)	t_w (mm)	H_w (m)	L_w (m)	FM **
61		5	1:2	–		0	92	1.42	2.13	DK
62		3	1:2	–		0	92	1.42	2.13	DK
63		6	1:2	V		48	92	1.42	2.13	SS
64		7	1:2	–		0	92	1.42	2.13	CC
65		8	1:2	V		48	92	1.42	2.13	DK
66		9	1:2	–		0	92	1.42	2.13	DK
67		10	1:2	V		48	92	1.42	2.95	SS
68		11	1:2	–		0	92	1.42	2.95	DK
69		12	1:2	–		0	92	1.42	2.95	DK
70	Suzuki et al. (2017)	1S-1B	1:4	V		58	48	0.71	1.16	CC
71		1S-1B-V	1:4	H		58	48	0.71	1.16	CC
72	Misir et al. (2016)	AWF	4:5	–	AAC-B	0	200	2	3.2	CC
73	Schwarz et al. (2015)	1000	1:2	–		0	100	1.4	0.9	–
74		1100	1:2	–		0	100	1.4	0.9	–
75		0000	1:2	–		0	100	1.4	2.05	–
76		0100	1:2	–		0	100	1.4	2.05	–

Table 1 (continued)

#	References	Label	Scale	Holes*	Bt	Void (%)	t_w (mm)	H_w (m)	L_w (m)	FM **
77		0101	1:2	–		0	100	1.4	2.05	–
78	Zhai et al. (2016)	2	1:1	V		55	190	2.6	2.8	DC
79	Zovkic et al. (2013)	Model 3	1:2	–		0	120	1.3	1.8	–

Bt = brick typology, t_w = infill wall thickness, H_w = infill wall height, L_w = infill wall length

S-Cl-B = solid clay bricks, H-Cl-B = hollow clay bricks, NC-B = normal concrete blocks, AAC-B = aerated autoclaved blocks

*Holes' direction, H = horizontal, V = vertical

**FM = failure mode, CC = corner crushing, SS = sliding shear, DK = diagonal cracking, DC = internal crushing, – not available

†Test performed by the authors of this work in the laboratory of DIST at University of Naples Federico II

Table 2 Collected database of infilled RC frames with openings

#	References	Label	Scale	Holes*	Bt	FM**	Void (%)	t_w (mm)	H_w (m)	L_w (m)	A_{op}/A_w (–)	x/L_w (–)
80	Mansouri et al. (2014)	DO	1:2	–	S-Cl-B	DC + SS	0	106	1.30	2.10	0.16	0.20
81		RWO	1:2	–		DC + SS	0	106	1.30	2.10	0.16	0.00
82		LWO	1:2	–		DC + SS	0	106	1.30	2.10	0.27	0.00
83		EWO	1:2	–		DC + SS	0	106	1.30	2.10	0.16	0.20
84	Stavridis (2009)	CU2	2:3	–		SS	0	95	1.86	3.38	0.11	0.10
85		CU5	2:3	–		SS	0	95	1.86	3.38	0.16	0.09
86		CU6	2:3	–		SS	0	95	1.86	3.38	0.18	0.09
87	Velazquez-Dimas et al. (2012)	BMWWR	2:3	–		DC	0	130	2.10	3.00	0.19	0.00
88	Kakaletsis (2009)	WX1	1:3	H	H-Cl-B	DC	36	60	0.80	1.20	0.10	0.33
89		WX2	1:3	H		DC	36	60	0.80	1.20	0.10	0.17
90	Kakaletsis and Karayannis (2007, 2008, 2009)	DO2	1:3	H		DC	36	60	0.80	1.20	0.20	0.00
91		WO2	1:3	H		SS	36	60	0.80	1.20	0.10	0.00
92		WO3	1:3	H		SS	36	60	0.80	1.20	0.24	0.00
93		WO4	1:3	H		SS	36	60	0.80	1.20	0.21	0.00
94		DO3	1:3	H		DC + SS	36	60	0.80	1.20	0.30	0.00
95		DO4	1:3	H		DC + SS	36	60	0.80	1.20	0.40	0.00
96		DX1	1:3	H		–	36	60	0.80	1.20	0.20	0.33
97	Sigmund and Penava (2012)	I/1	1:2	V		SS	55	120	1.30	1.80	0.13	0.00
98		I/2	1:2	V		SS	55	120	1.30	1.80	0.13	0.00
99		I/3	1:2	V		SS	55	120	1.30	1.80	0.13	0.28
100		I/4	1:2	V		SS	55	120	1.30	1.80	0.13	0.24
101	Velazquez-Dimas et al.(2012)	HBMW	2:3	–	NC	DC	–	120	2	3	0.19	0.00

Table 2 (continued)

#	References	Label	Scale	Holes*	Bt	FM**	Void (%)	t_w (mm)	H_w (m)	L_w (m)	A_{op}/A_w (–)	x/L_w (–)
102	Schwarz et al. (2015)	0010	1:2	–	AAC-B	–	0	100	1.4	2.05	0.11	0.00
103		0110	1:2	–		–	0	100	1.4	2.05	0.11	0.00
104	Zhai et al. (2016)	3	1:1	V		–	55	190	2.6	2.8	0.20	0.00
105		4	1:1	V		–	55	190	2.6	3.6	0.20	0.00

Bt = brick typology, t_w = infill wall thickness, H_w = infill wall height, L_w = infill wall length

S-Cl-B = solid clay bricks, H-Cl-B = hollow clay bricks, NC-B = normal concrete blocks, AAC-B = aerated autoclaved blocks

*Holes' direction, H = horizontal, V v= ertical

**FM = failure mode, CC = corner crushing, SS = sliding shear, DK = diagonal cracking, DC = internal crushing, - not available

by a slenderness ratio (H_w/t_w) ≤ 15, whereas more than 90% of the collected infill panels are characterized by an aspect ratio (L_w/H_w) > 1. Furthermore, bricks without holes constitute approximately 40% of all the considered infill panels; the remaining part is almost uniformly distributed between horizontal and vertical holes directions. In particular, slightly more than 50% of panels with hollow clay bricks are characterized by horizontal holes direction, while vertical holes are the most common for concrete blocks.

Finally, note that a limited number of tests are available on infilled RC frames with openings (Table 2). A database of 26 tests on infills with doors (7 tests) or windows (19 tests) characterized by a comprehensive description of damage evolution has been found in the literature. More specifically, scaled tests with both doors and windows are considered, characterized by opening percentages (void-to-total infill area, A_{op}/A_w), ranging between 10 and 40% (see Table 2) and infill slenderness ratios (H_w/t_w) between 10.8 and 19.6. Opening eccentricity, which is defined as the ratio between the horizontal distance between the midpoint of the opening length and the midpoint of the infill length (x) and the infill length itself (L_w), ranges between zero and 0.33 for the collected tests (see Table 2). Notably, no ties or other steel reinforcements are present around the openings for all the tests belonging to the database.

The experimentally observed failure mode (FM), according to the definition by Bertoldi et al. (1993), is also shown in Tables 1 and 2 for each test.

Table 3 reports the statistics (16th, 50th, and 84th percentiles) of the main mechanical properties (infill compressive strength, f_{pme}, and infill Young's modulus, E_m) related to the categories defined in Fig. 1. The variability ranges obtained from these statistics define the applicability thresholds of this work.

3 Damage analysis

Starting from the analysis of damage evolution under increasing drift demand for the collected tests, the drift capacities at given performance levels have also been identified as explained in this section. Then, fragility curves at different DSs are proposed depending on the brick material and, when possible, on the main mechanical and geometrical properties.

3.1 Definition of DSs and collected data

Some different definitions of DSs have been proposed in the literature in recent years, as was briefly mentioned in Sect. 1. Among these DSs, those proposed by the AeDES survey form (Baggio et al. 2007) are particularly important in the Italian framework. The latter aims to determine post-earthquake damage assessment for ordinary buildings, to determine short-term countermeasures to apply and to provide a usability judgement through a quick and visual survey. Recently, such results have been used in Italy to properly address repair actions and funds for reconstruction.

More specifically, Baggio et al. (2007) defined three DSs reporting an accurate and detailed damage description with a quantitative indication of crack widening for each DS. More recently, Cardone and Perrone (2015) reported a definition of DSs similar to those of the AeDES survey forms (see Table 4), adding a further DS. Indeed, DS1 (*light cracking*) and DS2 (*extensive cracking*) are very similar to those defined in the AeDES form, reporting further indications about the width of diagonal cracks (widespread crushing and

Table 3 Variability ranges of infill compressive strength (f_{pme}) and infill Young's modulus (E_m) for the categories defined in Fig. 1

Presence of openings	Category	Brick typology	16prctile E_m (MPa)	50prctile E_m (MPa)	84prctile E_m (MPa)	16prctile f_{pme} (MPa)	50prctile f_{pme} (MPa)	84prctile f_{pme} (MPa)
All	All	All	670	1700	7975	2.42	3.50	11.42
Without openings	All	All	1090	2355	8100	2.45	4.60	11.44
	Clay bricks	H-Cl-B	1090	1688	3991	2.24	3.56	5.35
		S-Cl-B	1700	2356	7450	3.76	5.20	10.96
	Concrete blocks	NC-B	4597	8234	11,081	9.66	13.45	18.29
		AAC-B	107	107	1335	2.50	2.70	2.70
With openings	All	All	670	858	3900	2.30	2.63	2.70
	Clay bricks	H-Cl-B	670	670	3900	2.63	2.63	2.70
		S-Cl-B	437	934	7975	2.30	2.45	14.50
	Concrete blocks	NC-B	2255	2255	2255	4.10	4.10	4.10
		AAC-B	1045	1265	1485	1.90	2.30	2.70

C = concrete, Cl = clay, S-Cl-B = solid clay bricks, H-Cl-B = hollow clay bricks, NC-B = normal concrete blocks, AAC-B = aerated autoclaved concrete blocks

Table 4 Adopted DSs definition and comparison with AeDES form

Damage state	AeDES form (Baggio et al. 2007)	Damage state	Adopted (Cardone and Perrone 2015)
D1 light damage	Cracks up to 2 mm due to separation of the infill walls from the structures, slight diagonal cracks in the infills (< 1 mm)	DS1 light cracking	Detachment between the masonry panel and RC frame Light diagonal cracking of the infill (1–2 cracks with widths < 1 mm) in both directions
D2–D3 medium-severe damage	Significant separations from the structure (2–5 mm), diagonal cracks or displacements of a few mm, visible crushing at the infill corners	DS2 extensive cracking	The cracks developed at DS1 widen (1 mm < width < 2 mm). New diagonal cracks are expected to appear in both directions (25–35% of the panel area). Possible failure of some brick units located on the upper corners and top edge of the infill (corresponding to 10% of the panel area)
D4–D5 collapse	Total collapse of infill panels	DS3 corner crushing	Detachment of large plaster area and significant sliding in the mortar joints Crushing and spalling of brick units (30% of the panel area)
		DS4 collapse	In-plane or out-of-plane (whichever occurs first) global collapse of the wall

spalling of brick units in up to 30% of the panel area), and DS4 (*collapse*) to the in-plane or out-of-plane (whichever occurs first) global collapse of the infill panel.

In this study, starting from the analysis of damage evolution and extensions of the collected infill panels, the definition of DSs is assumed as reported in Table 4. Furthermore, a certain degree of correspondence can be found between DSs adopted herein and limit states definitions by technical codes worldwide (Sassun et al. 2016), as explained below.

A commonly accepted definition of DSs specifically related to performance levels of infills does not yet exist in the literature. International codes generally define some limit states (or performance levels, PLs) to perform safety checks without providing any objective quantification of the acceptable damage level at each limit state. In particular, in the European region, Eurocode 8 (CEN 2005) considers two main PLs: damage limitation (DL) and life safety (LS) PLs. In more detail, according to Eurocode 8 (CEN 2005), at DL PL *the structure shall be designed and constructed to withstand a* given *seismic action […] without the occurrence of damage and the associated limitations of use, the costs of which would be disproportionately high in comparison with the costs of the structure itself*. This concept is also confirmed, with a slightly more restrictive vision, in Italian D.M. (2008) for the same limit state, where DL PL is associated with a limit of the temporary interruption of the structures' use (to perform some non-time-consuming and economic repair actions). Therefore, it appears reasonable to assume that, at DL PL, the damage to infills should be easily and economically repairable, as it appears until DS2 is attained, according to the definition adopted herein.

On the other hand, at LS PL, the structure should maintain its structural integrity and residual load bearing capacity (CEN 2005). It should be verified that nonstructural elements, and thus also masonry infills, do not represent a danger for LS, likely due to the spalling of some brick units. Therefore, it can be assumed that at LS PL an infill panel should have a residual capacity against its collapse (the latter likely occurring at DS4), even if its reparability is not economically convenient; namely, LS PL could be associated with DS3 (see also Sect. 5), as adopted in this study.

In addition, the Italian D.M. (2008) also defines the operational limit state and the near collapse limit state. The former corresponds to cosmetic damage that does not preclude the use of the structure and is therefore associated with the definition of DS1 adopted herein. The latter is characterized by serious damage to the structures and the collapse of nonstructural components, as identified in DS4 for infills.

Notably, given the definition of the DSs, each DS can be achieved in different ways, namely, due to different types of preeminent damage. For instance, infill achieves DS2 when (i) extensive cracks spread within the infill panel in both directions in approximately 30% of the panel area or when (ii) possible failure of brick units at the corners occurs in 10% of the total infill area. Therefore, the attainment frequency of each DS can be evaluated depending on the prevalent, observed damage for the collected tests with solid panels. As a result, DS2 is generally achieved (88% of tests) due to extensive cracks in the diagonal directions, and only in 12% of cases DS2 is attained due to brick failure at the corners. Similarly, DS1 is generally attained due to the occurrence of first hairline cracks in the panel. At DS3, crushing or spalling of brick units (30%) and significant sliding in mortar joints have approximately the same frequency of occurrence. Finally, DS4 always occurs due to in-plane collapses, as experimental tests properly dedicated to the out-of-plane collapse are not considered in this study. The attainment of this last damage level is generally described and declared by the authors of the experimental campaigns or obtained by attaining a constant residual branch in the in-plane response of the infill panel or of the infilled frame. In approximately 15% of tests, IDR at DS4 is assumed to be coincident with the end

of the test due to the lack of specific, useful information, thus representing a lower bound for the actual attainment of that DS. These observations could be useful in loss estimation when specific repair activities for each DS must be considered, also depending on the preeminent damage pattern of the infill (see Sect. 5).

On the other hand, the analysis of experimental tests on panels with openings shows that the damage pattern evolution under increasing drift levels is slightly different with respect to solid panels. In particular, it was observed that the detachment of the infill panel from the frame generally occurs first; then, the first inclined cracks in the piers lateral to the openings appear together with the occurrence of bed joint sliding in the portion above the opening. Note also that first inclined cracks generally appear first near the corners of the openings, where for increasing drift levels, crushing and consequent spalling of brick units also occur, until the total collapse of the infill wall.

Tables 5 and 6 show the IDR values obtained at each DS for each specimen without and with openings, respectively.

Notably, some experimental works from the literature (see, e.g., Petry and Beyer 2014; Frumento et al. 2009) determined how the unit-to-wall size ratio can potentially influence the experimental response of unreinforced masonry walls, particularly referring to higher in-plane drift capacity. In particular, a decreasing trend in drift capacities was observed with increasing unit-to-wall size ratio. On this basis, the use of relatively scaled infills with full-scale size units could potentially affect damage patterns and drift capacity. Nevertheless, these studies were related to unreinforced masonry walls instead of masonry infills with a surrounding RC frame. In addition, no information has been found in the literature regarding such an influence at lower drift levels or on unreinforced masonry walls.

The available data on infilled frames belonging to the collected database do not allow for evaluation of the size effect influence on drift capacity at each damage state because no experimental study has been found that specifically analysed this effect. Such a topic is certainly worth investigating in the future. In the collected database, approximately 75% of tests are 1:2 scale infilled frames. Few tests were performed on full-scale specimens. Often, when a scale factor equal to or lower than 1:2 is adopted, brick units are also adequately scaled (e.g., Akhound et al. 2015; Baran and Sevil 2010; Centeno et al. 2008; Kakaletsis and Karayannis 2007, 2008, 2009; Waly 2010; Suzuki et al. 2017). Based on this analysis of data and since the size effect issue can likely be more influential depending on the unit-to-wall size ratio, it can be argued that the possible influence of the size effect on drift capacity, if any, should be mitigated. Nevertheless, because of the lack of definite indications on this topic, supported by strong experimental evidence and to conservatively avoid excessive inhomogeneity within the database, tests with a particularly low scaling ratio, equal to 1:4 or 1:5 (Kyriakides and Billington 2008; Khoshnoud and Marsono 2016; Suzuki et al. 2017), have been discarded. Therefore, any bias in the analysed data due to possible scaling issues has likely been avoided.

3.2 Analysis of parameters influencing IDR capacity

The collected database includes specimens characterized by significant variability in different characteristics, namely, the brick typology (S-Cl-B, H-Cl-B, NC-B, AAC-B; see Sect. 2), an intratypology variability in geometrical and mechanical parameters. The possible influence of such variability in the IDR capacity at the analysed DSs will be investigated in this section by analysing the correlation between these parameters and IDR capacity. Generally, the inhomogeneity of the collected tests with respect to a parameter may

Table 5 IDR values at which each specimen reaches each DS without openings

#	Brick type	References	Specimen	DS1 (%)	DS2 (%)	DS3 (%)	DS4 (%)
1	S-Cl-B	Angel et al. (1994)	2a	0.17	0.34	–	–
2			3a	0.11	0.22	–	–
3			6a	0.13	0.25	–	–
4			7a	0.13	0.25	–	–
5			8a	0.20	0.39	–	–
6		Chiou and Hwang (2015)	B39L	0.13	0.50	0.75	2.00
7			B39T	0.13	0.50	0.75	2.00
8		Gazic and Sigmund (2016)	O3_cpm	0.17	0.53	–	1.35
9			O4_cpm	0.16	0.47	–	1.62
10			O1_cpm	0.17	0.40	–	1.70
11			O1_cvm	0.09	0.17	–	1.80
12			O2_cpm	0.16	0.44	–	0.99
13		*Khoshnoud and Marsono* (2016)	*F1*	*0.29*	–	*0.81*	*2.50*
14		*Kyriakides and Billington* (2008)	*1*	*0.09*	*0.43*	–	*1.94*
15		*Mansouri* et al. (2014)	*S*	*0.05*	–	–	*3.50*
16		Stavridis (2009)	CU1	0.05	0.23	–	0.74
17	H-Cl-B	*Baran and Sevil* (2010)	*SP9*	–	–	–	*3.25*
18		Bergami and Nuti (2015)	Ft1	0.16	0.70	1.30	–
19		*Cavaleri and Di Trapani* (2014)	*s1b2*	–	–	–	*1.53*
20		Colangelo (2005)	C1	0.03	–	–	1.42
21			C2	0.02	–	–	–
22			L1	0.03	–	–	1.63
23			L2	0.03	–	–	2.28
24			N1	–	–	–	2.03
25			N2	0.03	–	–	2.16
26		Gazic and Sigmund (2016)	O3_bpm	0.16	0.33	–	0.96
27			O4_bpm	0.18	0.29	–	0.94
28			O1_bpm	0.11	0.27	–	0.95
29			*O1_bvm*	*0.06*	*0.12*	–	*1.03*
30			O1_bpm*	0.05	0.29	–	0.94
31		Guidi et al. (2013)	URM_U	0.10	–	–	–
32		*Haider* (1995)	*A1*	*0.25*	*0.50*	*1.00*	*2.50*
33			*B1*	*0.25*	*0.50*	*1.00*	*2.50*
34			*D2*	*0.25*	*0.50*	*1.00*	*2.50*
35		Kakaletsis and Karayannis (2008)	S	–	0.28	–	1.90
36		Misir et al. (2016)	IWF	0.20	–	–	–
37		Morandi et al. (2014)	TA2	0.30	0.50	1.75	2.50
38		Sigmund and Penava (2012)	III/2	0.09	0.16	0.57	1.09
39		*Waly* (2010)	*2*	*0.22*	*0.58*	*1.71*	–
40		*Zarnic and Tomazevic* (1984)	*M2*	*0.11*	–	–	–

Table 5 (continued)

#	Brick type	Reference	Specimen	DS1 %	DS2 %	DS3 %	DS4 %
41		Zovkic et al. (2013)	Model 4	0.02	–	–	–
42			Model 8	0.02	–	–	–
43	H-Cl-B	Calvi and Bolognini (2001)	6	–	0.20	0.40	–
44		Colangelo (2005)	V11	0.02	–	–	2.21
45			V21	0.03	–	–	2.06
46			V22	0.03	–	–	2.26
47		DIST Unina	GI-120	0.15	0.50	1.30	1.70
48		*Misir* et al. (2016)	*SWF*	*0.35*	–	–	–
49		Pereira et al. (2011)	Ref_Wall	0.02	0.36	0.60	–
50		Ricci et al. (2017)	IP + OOP_L	0.07	–	–	–
51			IP + OOP_M	0.06	0.23	–	–
52			IP + OOP_H	0.07	0.23	0.43	–
53		Akhound et al. (2015)	MIF-I-2L	0.11	0.38	0.75	2.50
54		Verderame et al. (2016)	GI-80	0.15	0.50	1.30	1.70
55			SI-80	0.15	0.50	1.30	2.00
56	NC-B	Angel et al. (1994)	4a	0.05	–	–	–
57			5a	0.03	–	–	–
58		Centeno et al. (2008)	1	0.30	0.75	1.05	–
59		Crisafulli	Unit 1	0.08	0.30	1.50	–
60		Mehrabi et al. (1996)	4	–	0.17	0.99	–
61			5	–	0.33	1.32	–
62			3	–	0.21	–	–
63			6	–	0.36	0.91	–
64			7	–	0.46	0.86	–
65			8	–	0.2	1.49	1.80
66			9	–	0.33	0.82	–
67			10	–	0.17	0.91	–
68			11	–	0.36	0.91	–
69			12	–	0.17	0.66	–
70		Suzuki et al. (2017)	1S-1B	0.10	–	1.00	3
71			1S-1B-V	–	–	1.50	3
72	AAC-B	Misir et al. (2016)	AWF	0.20	–	–	–
73		Schwarz et al. (2015)	1000	0.33	1.33	–	2.67
74			1100	0.1	1	–	2.33
75			0000	–	–	–	2.67
76			0100	0.33	0.67	–	4
77			0101	–	–	1.33	–
78		Zhai et al. (2016)	2	0.11	–	0.86	1.43
79		Zovkic et al. (2013)	Model 3	0.06	–	–	–

S-Cl-B = solid clay bricks, H-Cl-B = hollow clay bricks, NC-B = normal concrete blocks, AAC-B = aerated autoclaved blocks

Italics represent the excluded cases to reduce inhomogeneity (as explained in Sect. 3.2)

Table 6 IDR values at which each specimen reaches each DS with openings

#	Brick type	Authors	Specimen	DS1 (%)	DS2 (%)	DS3 (%)	DS4 (%)
80	S-Cl-B	Mansouri et al. (2014)	DO	0.05	0.5	1.4	-
81			RWO	0.05	–	1	2.75
82			LWO	0.05	0.35	1	–
83			EWO	0.08	0.88	1.4	2.2
84		Stavridis (2009)	CU2	0.05	0.41	–	1.01
85			CU5	0.06	0.29	–	1.23
86			CU6	0.07	0.36	1	1.38
87		Velazquez-Dimas et al. (2012)	BMWWR	0.06	–	0.66	–
88	H-Cl-B	Kakaletsis (2009)	WX1	–	0.28	–	3.61
89			WX2	–	0.25	–	–
90		Kakaletsis and Karayannis (2007, 2008, 2009)	DO2	–	0.28	–	2.22
91			WO2	–	0.39	–	2
92			WO3	–	0.34	–	3
93			WO4	–	0.3	–	2.22
94			DO3	–	0.27	–	2.61
95			DO4	–	0.27	–	2.28
96			DX1	–	0.28	–	2.11
97		Sigmund and Penava (2012)	I/1	0.1	0.19	0.35	0.5
98			I/2	0.11	0.18	0.49	1.29
99			I/3	0.09	0.18	0.57	0.93
100			I/4	0.1	0.22	0.58	1.3
101	NC-B	Velazquez-Dimas et al. (2012)	HBMW	0.06	0.39	–	–
102	AAC-B	Schwarz et al. (2015)	10	–	–	–	2.8
103			110	–	–	–	2.67
104		Zhai et al. (2016)	3	–	0.8	1.87	3.02
105			4	0.27	–	1.6	2.13

S-Cl-B = solid clay bricks, H-Cl-B = hollow clay bricks, NC-B = normal concrete blocks, AAC-B = aerated autoclaved blocks

represent a critical issue and should therefore be properly considered, if this parameter is clearly and significantly correlated to the analysed IDR capacity values. In such a case, the fragility curves, whose derivation will be described in the subsequent section, can be properly specialized, i.e., a further clustering of the database is considered.

The first source of (geometrical) inhomogeneity is due to the presence of specimens with different scaling ratios; in this regard, although no clear indication is present in the literature, tests with a particularly low scaling ratio have been conservatively discarded (see Sect. 3.1). Furthermore, tests with an aspect ratio (L_w/H_w) lower than or equal to 1 (Haider 1995; Cavaleri and Di Trapani 2014) will also be discarded, since these tests represent a very minor part of the database. Therefore, the trend of the investigated IDR capacity within this range of values could not be reliably investigated based on the available data (see Sect. 2). Further tests were not considered for different reasons, namely, too high (Zarnic and Tomazevic 1984) or too low (Mansouri et al. 2014; test "O1_bvm" by Gazic and Sigmund (2016)) values of infill compressive strength, compared to the remaining tests, or

no information regarding infill compressive strength (Baran and Sevil 2010), or the presence of two infill layers with different thicknesses and therefore, the impossibility of defining a unique slenderness value for the panel (Misir et al. 2016). These excluded tests are highlighted in grey in Table 5.

Among the potential influencing parameters, the following are selected because previous studies and/or mechanical-based considerations indicate the influence of these parameters on the response of the panel or their possible direct correlation with the panel's IDR capacity at different DSs (or Limit States).

Regarding the geometrical parameters, the slenderness ratio (H_w/t_w) and aspect ratio (L_w/H_w) are considered. A higher slenderness is expected to have a detrimental effect on the panel's response and thereby would also have a detrimental effect on IDR capacity due to possible out-of-plane instability of the panel. The influence of such a phenomenon on the panel's strength has already been considered by other authors (e.g., Saneinejad and Hobbs 1995). The aspect ratio can influence the IDR capacity since, given equal IDR demand, panels with different values of L_w/H_w are characterized by different strain demands in the diagonal compressive strut (e.g., Hak et al. 2012).

Furthermore, the interaction between the panel and surrounding elements is recognized to have a significant influence on the panel's response; this interaction can be effectively analysed through relative panel-to-frame stiffness and strength ratios (Alwashali et al. 2018). The former is usually and commonly expressed through the λh parameter (Stafford Smith 1962), which is directly linked to the width of the equivalent diagonal strut in different modelling approaches (Chrysostomou and Asteris 2012). The latter can be expressed through the strength ratio parameter (V_{RC}/V_w), which is already adopted (alongside L_w/H_w) by the ASCE/SEI 41 standard (ASCE 2013) for predicting the deformation capacity of the panel at LS. When evaluating this strength ratio, the expected frame strength (V_{RC}) is calculated assuming a plastic mechanism in the frame columns (ASCE 2013), and the expected infill strength (V_w) is calculated as the product between the infill shear cracking strength and the infill area. The latter approach was observed to provide a strength prediction very close to that of the experimental observations based on a dataset of tests on hollow clay masonry infills (De Risi et al. 2018).

The analysis of the influence of these parameters on IDR capacity at the considered DSs will be conducted within the clay bricks (Cl-B) typology (without openings), since the higher number of tests allows for a more significant and reliable investigation of the analysed trends.

The influence of the slenderness ratio (H_w/t_w) is first analysed (see Tables 7, 8). This parameter shows significant variability (coefficient of variation, CoV, is equal to 33% and 53% for subsets H-Cl-B and S-Cl-B, respectively), both within the H-Cl-B and S-Cl-B

Table 7 Statistics of main geometrical and mechanical parameters and correlation with IDR capacity within the hollow clay bricks (H-Cl-B) typology

H-Cl-B	Main statistics					Correlation coefficients			
	Min	Max	Mean	Median	CoV (%)	DS1	DS2	DS3	DS4
H_w/t_w	8.4	23.9	13.7	11.3	33	−0.29	−0.38	−0.54	0.41
L_w/H_w	1.28	2.06	1.53	1.50	13	−0.23	0.40	−0.07	0.62
λh	1.56	5.11	2.66	2.41	30	0.09	−0.22	−0.22	−0.59
V_{RC}/V_w	0.19	3.58	1.38	1.31	56	−0.18	−0.65	−0.83	−0.09

Table 8 Statistics of main geometrical and mechanical parameters and correlation with IDR capacity within the solid clay bricks (S-Cl-B) typology

S-Cl-B	Main statistics					Correlation coefficients			
	Min	Max	Mean	Median	CoV (%)	DS1	DS2	DS3	DS4
H_w/t_w	8.7	34.1	16.2	13.2	53	−0.20	−0.43	–	−0.47
L_w/H_w	1.42	2.58	1.73	1.69	23	−0.23	0.30	–	0.47
λh	1.81	3.57	2.88	3.42	68	−0.17	0.47	–	−0.75
V_{RC}/V_w	0.27	3.57	1.20	0.83	26	0.32	−0.18	–	0.53

typologies. A significant negative correlation is observed at all DSs in both cases, except DS4 for H-Cl-B and DS3 for S-Cl-B (for which only one value is present). Hence, this dependence will be considered in the derivation of fragility curves reported below (see Sect. 3.3).

The influence of the aspect ratio (L_w/H_w) shows different trends. First, this parameter is relatively less variable within the considered subsets (CoVs equal to 13% (H-Cl-B) and 23% (S-Cl-B), as shown in Tables 7 and 8, respectively). Then, the correlation with the IDR capacity is unclear and inconsistent between the different DSs. Hence, no further database clustering will be conducted depending on the L_w/H_w in the following. The influence of L_w/H_w on the deformation capacity was also analysed by Turgay et al. (2014) and Alwashali et al. (2018) based on tests collected from the literature. Turgay et al. (2014) analysed the IDR capacity at "yielding" (corner of a bilinear envelope approximating the lateral response of the infilled frame) and at "ultimate" IDR (15% loss of lateral strength); these researchers found that the latter was negatively correlated with L_w/H_w, but the too high scatter made it impossible to draw reliable conclusions. Similarly, Alwashali et al. (2018) analysed the IDR capacity at cracking, maximum and "ultimate" (20% lateral strength loss) in the multilinear envelope approximating the lateral response of the infilled frame, and these researchers observed no clear trend in the IDRs at maximum and ultimate with L_w/H_w. Conversely, the ASCE/SEI 41 standard (ASCE 2013) assumes a decreasing trend of the IDR capacity (at LS LS) with increasing L_w/H_w.

The stiffness ratio (λh) does not show a significant correlation with the IDR capacity, and no clear and consistent trend is observed, especially at low DSs (DS1 and DS2) (see Tables 7, 8). The λh parameter is calculated according to Stafford Smith (1962) by using the initial (gross) flexural stiffness for the RC columns and the initial (pre-cracking) Young's modulus (E_m) for the masonry panel. Therefore, from a theoretical point of view, a significant correlation between this parameter and the IDR capacity should be expected, especially at DSs closer to the IDR range at which the RC elements and the infill panel are still in their elastic range, or slightly beyond, i.e., at DS1 and DS2. Nevertheless, contrary to this consideration, no clear trend is observed, especially at low DSs, as mentioned above. These considerations apply to both H-Cl-B and S-Cl-B. Hence, it will not be considered as a further predictive parameter.

Finally, the influence of the strength ratio V_{RC}/V_w is analysed. This parameter is considered only within the H-Cl-B subset because complete information on the characteristics of surrounding elements is not always available for S-Cl-B, resulting in a low number of tests. At all DSs, a negative correlation is observed between V_{RC}/V_w and IDR capacity (Tables 7, 8). This correlation is stronger at DS2 and DS3, i.e., at DSs likely closer to the IDR range at which both the panel and the surrounding frame are expected to develop

their peak strength, which appears reasonable. Such trends do not agree with the provisions of ASCE/SEI 41 (ASCE 2013), which assumes an increasing IDR capacity at the LS Limit State with increasing V_{RC}/V_w, referring to range of values delimited by 0.7 and 1.3. Turgay et al. (2014) found that ASCE/SEI 41 IDR limits represented a safe lower bound for the "ultimate" IDR (as defined by the authors) up to $V_{RC}/V_w = 1.3$, but not for higher values. Alwashali et al. (2018) found that the "ultimate" IDR increased with increasing V_{RC}/V_w, which is consistent with the ASCE/SEI 41 provisions; however, these provisions represented a safe lower bound for the observed values. Notably, a comparison between the findings of these studies, ASCE/SEI 41 provisions and the results of the present work are not fully consistent, due to the differences in the adopted definitions of DSs (e.g., corresponding to assumed percentages of lateral strength loss), which do not allow for direct comparison.

3.3 Drift-based fragility curves

For each DS, the empirical cumulative distribution (ECD) of IDR is obtained by plotting ascending-ordered drift ratio values against $(i-0.5)/n$, where "i" is the position of the drift ratio value in the ordered list of drift ratios and "n" is the total number of drift values for that damage state. The ordered data have also been revised to delete possible spurious values, which reflect experimental errors or misinterpretation of experimental results. To this end, Peirce's criterion (Ross 2003) has been applied, and potential doubtful observations of IDR values have been deleted, as suggested by FEMA-P58. Then, the method of maximum likelihood was used to fit ECDs with a lognormal fragility function (LN_CDF), which is typical in these applications. A lognormal fragility function is fully defined by only two statistical parameters, as shown in Eq. (1).

$$\mathrm{LN\_CDF}\left(\mathrm{DS} \geq \mathrm{ds_i} \middle| \mathrm{IDR_j}\right) = \Phi\left(\frac{\ln\left(\mathrm{IDR_j}\right) - \mu_i}{\beta_i}\right) \tag{1}$$

where $\mathrm{LN\_CDF}(\mathrm{DS} \geq \mathrm{ds_i}|\mathrm{IDR_j})$ is the conditional probability that the component will experience or exceed the ith damage state given the inter-story drift value $\mathrm{IDR_j}$; $\Phi(\cdot)$ is the standard normal cumulative distribution function; (μ_i) is the logarithmic mean value; and (β_i) is the logarithmic standard deviation. The ECDs and LN_CDFs for the four DSs are shown in Fig. 2. Note that the total dispersion, β_i, represents the uncertainty in the actual

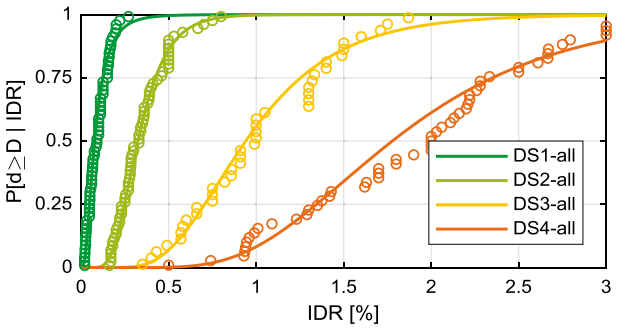

Fig. 2 Proposed fragility function curves for infill panels (all data)

Table 9 Number of available data and parameters for fragility curves (all data)

	N	DS1			DS1			DS1			DS1		
		e^{μ}	β_r	β	e^{μ}	β_r	β	e^{μ}	β_r	β	e^{μ}	β_r	β
All data	94	0.08	0.10	0.70	0.32	0.10	0.40	0.94	0.10	0.40	1.78	0.10	0.40

value of IDR at which a damage state is likely to start. If fragility curves are obtained based on a limited set of experimental data, two sources of uncertainty should be considered. The first one ($\beta_{r,i}$) represents the random variability observed in the collected data from which the fragility parameters are calculated. The second source ($\beta_{u,i}$) represents uncertainty in the difference between testing specimens/procedures and actual installation/loading conditions, or uncertainty that the available data represent an adequate sample size to accurately represent the true random variability (FEMA P-58 2012b). The total dispersion at the ith DS, (β_i), is finally computed as the square root of the sum of squares of $\beta_{r,i}$ and $\beta_{u,i}$, as shown in Eq. (2):

$$\beta_i = \sqrt{\beta_{r,i}^2 + \beta_{u,i}^2} \tag{2}$$

When all data are used together to obtain the fragility curves presented in Fig. 2, ($\beta_{u,i}$) is assumed to be equal to 0.10 for each DS, according to FEMA-P58. Otherwise, the value of ($\beta_{u,i}$) is assumed to range between 0.10 and 0.40, mainly depending on the sample size of the available data (FEMA-P58, Lowes and Li 2011), as shown in the subsequent sections, where all the collected data will be divided into homogeneous data subsets. In summary, the resulting median drift capacity (e_i^{μ}) for each DS and the total number of tests (N) are reported in Table 9. Logarithmic standard deviations of LN_CDFs (i) that come from the available data ($\beta_{r,i}$) and (ii) obtained through Eq. (2) (approximated to the first decimal place) are also reported.

The values of e^{μ} evaluated herein (shown in Table 9) are generally lower than the corresponding values reported in (Cardone and Perrone 2015), especially at DS1 (−47%) and DS2 (−20%); closer values of e^{μ} are obtained at DS3 (−6%) and DS4 (+2%). Similar trends can be observed if median capacity drifts obtained herein are compared with the corresponding results of Sassun et al. (2016). Values of logarithmic standard deviations, β, are generally higher at less severe DSs, especially at DS1, and generally higher than those in previous studies. These differences can be mainly justified based on (i) the different amounts of adopted data (see Sect. 2) and (ii) the "purely observational" approach adopted in the present work. Conversely, a hybrid approach is adopted in other studies from the literature by integrating observed damage evolution and characteristic points of the infilled frame in-plane response (Cardone and Perrone 2015) or the infill panel (Del Gaudio et al. 2017; De Risi et al. 2017). The values of e^{μ} shown in Table 9 are also quite similar to those proposed in (Colangelo 2013), except at DS1, where the median drift capacity proposed herein is approximately three times higher than that proposed in (Colangelo 2013). High values of β were also found in (Colangelo 2013), ranging between 24 and 97%.

In the following discussion, all the data analysed so far will be classified into homogeneous subsets. First, in Sect. 3.3.1, data related to tests without openings, which represent the major part of the collected database, will be divided depending on the brick material (clay or concrete), the typology of brick units, and main influential geometrical and mechanical parameters as remarked in Sect. 3.2. Then, some remarks about the presence of openings

are made (Sect. 3.3.2). In such a way, the influence of these "variables" on the fragility curves shown in Fig. 2 can be investigated, and more specific curves can be derived for further applications, such as a more refined analysis of losses due to earthquakes for infilled RC buildings depending on the infill typology and properties (see Sect. 5).

3.3.1 Infills without openings

In this section, tests without openings are considered first, and the same procedure explained above is applied to obtain the related fragility curves. The resulting parameters e_i^{μ} and β_i are reported in Table 10 (first row). The fragility parameters obtained in this case are very similar to those calculated and shown in Table 10, due to the significant number of tests without openings within the entire dataset.

Then, all these data points are classified depending on the brick material typology to quantify the influence of such a parameter on the drift-based fragility curves. To this end, infills with clay bricks and tests with concrete blocks are considered separately to calculate the parameters of the related fragility curves (see the second and the fifth rows of Table 10 and Fig. 3a). The infills with concrete blocks (C-B) exhibit median drift capacities that are generally higher than the corresponding values related to infills with clay bricks (Cl-B) at each DS (see Table 10). In particular, at DS4, the median drift capacity for infills with concrete blocks is +57% higher than for infills with clay bricks (2.50 vs. 1.59). The only exception appears with DS2, at which the drift capacity of clay and concrete bricks are very close to each other (0.33). However, the drift capacity increment for concrete blocks is equal to +31% with respect to clay bricks, considering all the DSs on average. Additionally, values of logarithmic standard deviation are comparable between these two classes (Table 10).

A further material-based classification is also shown in Table 10. Fragility curves for solid clay bricks (S-Cl-B) and hollow clay bricks (H-Cl-B) have been obtained starting from all data tests related to clay bricks (see the third and fourth rows), whereas fragility curves for normal concrete blocks (NC-B) and autoclaved aerated concrete blocks (AAC-B) have been derived for the typology "concrete blocks" (see the sixth and seventh rows). The related fragility curves are shown in Fig. 3b, c. A slight drift capacity reduction is generally observed passing from hollow bricks to solid bricks, except at DS1 (see Table 10, Fig. 3b). More specifically, solid bricks exhibit a higher drift capacity at DS1 (more than double with respect to hollow clay bricks), whereas less significant variations (decrements) are observed at the remaining DSs. Again, at DS2, fragility curves related to hollow and solid clay bricks are very close to one another. Finally, AAC blocks generally show higher drift capacity with respect to NC blocks (see Table 10, Fig. 3c). Nevertheless, tests regarding AAC infills are rarely cited in the literature due to their most recent diffusion in real RC buildings; therefore, few data are generally available for this data subset. In fact, only two data points have been collected at DS3, thus making a fragility curve proposal for that DS not feasible. Finally, only at DS4, AAC-B and NC-B exhibit approximately the same drift capacities. Notably, a great difference between NC-B and AAC-B exists. In particular, considering the collected tests, Young's modulus and infill compressive strength are more than ten times lower and five times lower, respectively, for AAC-B with respect to concrete blocks on average. This evidence could justify the significant difference between fragility curves for AAC-B and NC-B, especially at lower DSs such as DS1 and DS2.

A further classification of experimental data has been conducted considering the investigation presented in Sect. 3.2, particularly for the H-Cl-B and S-Cl-B subsets. Therefore,

Table 10 Number of available data and parameters for fragility curves depending on brick typology

w/o openings	N	DS1			DS2			DS3			DS4		
Subset		e^{μ}	β_r	β	e^{μ}	β_r	β	e^{μ}	β_r	β	e^{μ}	β_r	β
All	68	0.08	0.80	0.80	0.33	0.42	0.40	0.97	0.39	0.40	1.72	0.37	0.40
Clay	44	0.08	0.81	0.80	0.33	0.37	0.40	0.89	0.49	0.50	1.59	0.35	0.40
Hollow bricks (H-Cl-B)	31	0.06	0.85	0.90	0.33	0.37	0.40	0.92	0.52	0.60	1.65	0.35	0.40
Solid bricks (S-Cl-B)	13	0.14	0.22	0.50	0.34	0.36	0.40	0.75	–	0.40	1.45	0.33	0.40
Concrete	24	0.11	0.78	0.80	0.33	0.56	0.60	1.04	0.25	0.40	2.50	0.3	0.40
Normal blocks (NC-B)	16	0.06	0.45	0.60	0.26	0.35	0.50	1.04	0.25	0.40	2.53	0.24	0.50
Aerated autoclaved (AAC-B)	8	0.15	0.66	0.70	0.96	0.29	0.50	–	–	–	2.49	0.33	0.50

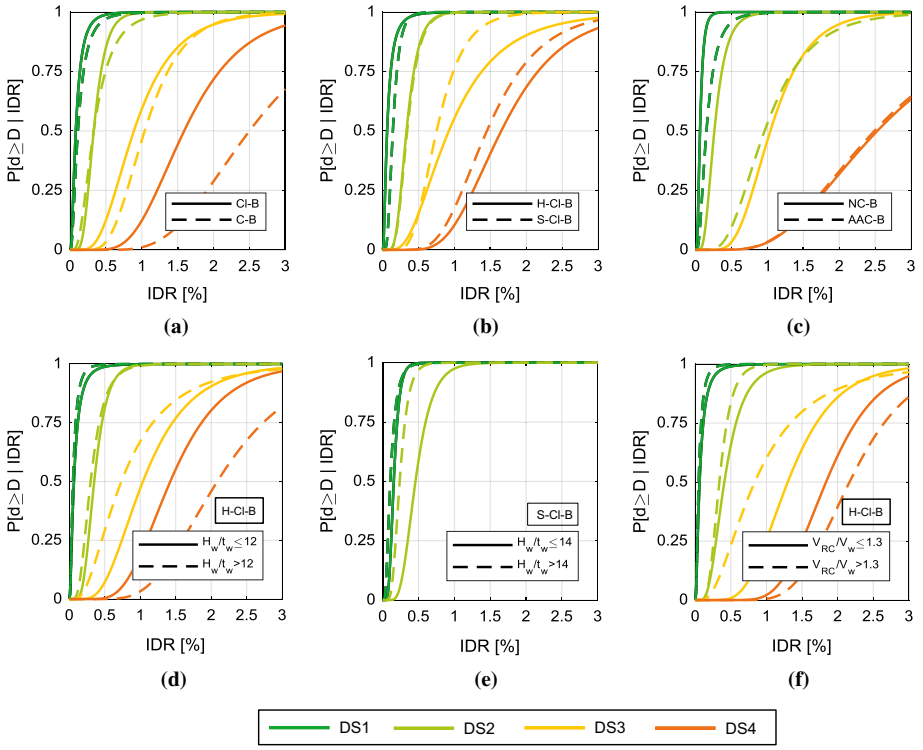

Fig. 3 Fragility functions for infills depending on brick material: clay bricks (Cl-B) and concrete blocks (C-B) (**a**), hollow clay bricks (H-Cl-B) and solid (S-Cl-B) clay bricks (**b**), concrete blocks (NC-B) and autoclaved aerated concrete blocks (AAC_B) (**c**), fragility functions depending on slenderness: H-Cl-B specimens (**d**) and S-Cl-B infills (**e**), fragility functions depending on V_{RC}/V_w for H-Cl-B infills (**f**)

an additional clustering of the database has been performed, grouping data depending on (i) the slenderness ratio (H_w/t_w) and (ii) the relative strength ratio (V_{RC}/V_w), and the parameters most clearly affecting the drift capacity.

First, H-Cl-B specimens were grouped into two homogenous samples (with approximately the same number of data at each DS): tests characterized by H_w/t_w lower or equal to 12 (19 specimens) and tests with H_w/t_w greater than 12 (12 specimens). Similarly, for the S-Cl-B specimens, two samples were created: tests characterized by H_w/t_w lower or equal to 14 (8 specimens) and tests with H_w/t_w greater than 14 (5 specimens). Fragility curves, obtained by adopting the same methodology explained previously, have thus been properly specialized as a function of the slenderness ratio values. Table 11 shows the resulting parameters of these fragility curves as a function of H_w/t_w for the H-Cl-B and S-Cl-B subsets.

Figure 3d shows the fragility curves for the two clusters of H-Cl-B specimens depending on the slenderness ratio (H_w/t_w). On average, an increment of approximately 30% of median drift capacity exists at DS1–DS2–DS3 for lower slenderness ratios. DS4 is the only exception because a reduction in the median drift capacity of approximately 30% is observed in this case. Figure 3e reports the fragility curves for the two clusters of slenderness ratios for

Table 11 Number of available data and parameters for fragility curves depending on slenderness ratio and strength ratio for H-Cl-B and S-Cl-B subsets

w/o openings	N	DS1			DS2			DS3			DS4		
		e^{μ}	β_r	β	e^{μ}	β_r	β	e^{μ}	β_r	β	e^{μ}	β_r	β
H-Cl-B	31	0.06	0.85	0.90	0.33	0.34	0.40	0.92	0.52	0.50	1.65	0.35	0.40
$H_w/t_w \le 12$	19	0.07	0.90	0.90	0.35	0.31	0.40	1.04	0.45	0.50	1.42	0.39	0.40
$H_w/t_w > 12$	12	0.05	0.70	0.80	0.30	0.37	0.50	0.73	0.57	0.70	2.09	0.06	0.40
$V_{RC}/V_w \le 1.3$	13	0.06	0.84	0.90	0.41	0.41	0.50	1.30	–	0.40	1.84	0.16	0.30
$V_{RC}/V_w > 1.3$	14	0.05	0.80	0.80	0.34	0.33	0.40	0.84	0.53	0.70	2.17	0.13	0.30
S-Cl-B	13	0.14	0.22	0.50	0.34	0.36	0.40	0.75	–	0.40	1.45	0.33	0.40
$H_w/t_w \le 14$	8	0.15	0.15	0.40	0.46	0.11	0.40	–	–	–	1.73	0.14	0.40
$H_w/t_w > 14$	5	0.11	0.43	0.60	0.24	0.06	0.40	–	–	–	–	–	–

the S-Cl-B specimens. Notably, the fragility curves at DS3 and DS4 are not reported due to a lack of data. On average, an increment of approximately 70% of the median drift capacity at DS1 and DS2 is observed for lower slenderness ratio values.

Due to the effect of the relative strength ratio (V_{RC}/V_w) on the drift capacity (analysed in Sect. 3.2), a further clustering of the database has been conducted, grouping all the H-Cl-B tests in two additional homogenous subsets (with approximately the same number of data at each DS): tests characterized by V_{RC}/V_w lower than or equal to 1.3 (13 specimens) and tests characterized by V_{RC}/V_w greater than 1.3 (14 specimens). The influence of V_{RC}/V_w on the fragility curve parameters is thus evaluated. Fitting parameters of fragility curves for H-Cl-B as a function of V_{RC}/V_w are finally reported in Table 11. Corresponding fragility curves are finally shown in Fig. 3f. On average, an increment of approximately 35% of median drift capacity values for DS1–DS2–DS3 is observed for $V_{RC}/V_w \le 1.3$ with respect to the complementary subset. Conversely, a reduction in DS4 of approximately 15% is observed for lower values of V_{RC}/V_w.

3.3.2 Main remarks about the presence of openings

The analysis of the influence of door or window openings on damage assessment of infill panels is presented in this Section. First, the number of tests with openings is quite limited with respect to tests without openings, as already discussed in Sect. 2. However, the experimental campaigns that address infills with openings also generally analyse a benchmark test. For each experimental campaign, the benchmark test is equal to the other tests, except that it is infilled by a solid panel (without openings). This peculiar condition, which is unlikely to occur for other parameters affecting infill performance, makes the analysis of the influence of openings possible starting from each single experimental campaign, by only comparing drift capacity of such a "reference solid" panel and the corresponding infills with doors or windows openings. The ratios Ω between the IDR capacity of each specimen with openings and its corresponding "reference solid" test are reported in Table 12.

Table 12 Ω ratios for each experimental campaign

No.	Brick type	Authors	Specimen	With openings/no openings (Ω)			
				DS1	DS2	DS3	DS4
80	S-Cl-B	Mansouri et al. (2014)	DO	1.00	–	–	–
81			RWO	1.00	–	–	0.79
82			LWO	1.00	–	–	–
83			EWO	1.50	–	–	0.63
15			S	Reference solid			
84		Stavridis (2009)	CU2	1.00	1.78	–	1.36
85			CU5	1.28	1.24	–	1.66
86			CU6	1.38	1.57	–	1.86
16			CU1	Reference solid			
88	H-Cl-B	Kakaletsis (2009)	WX1	–	1.01	–	1.90
89			WX2	–	0.91	–	–
35			S	Reference solid			
90		Kakaletsis and Karayannis (2007, 2008, 2009)	DO2	–	0.99	–	1.17
91			WO2	–	1.38	–	1.05
92			WO3	–	1.21	–	1.58
93			WO4	–	1.07	–	1.17
94			DO3	–	0.96	–	1.37
95			DO4	–	0.96	–	1.20
96			DX1	–	1.00	–	1.11
35			S	Reference solid			
97		Sigmund and Penava (2012)	1	1.11	1.19	0.61	0.46
98			2	1.22	1.13	0.86	1.18
99			3	1.00	1.13	1.00	0.85
100			4	1.11	1.38	1.02	1.19
38			2/III	Reference solid			
102	AAC-B	Schwarz et al. (2015)	0010	–	–	–	1.05
75			0000	Reference solid			
103			0110	–	–	–	0.67
76			0100	Reference solid			
104		Zhai et al. (2016)	3	1.91	–	2.18	2.11
105			4	2.45	–	1.87	1.49
78			2	Reference solid			

S-Cl-B = solid clay bricks, H-Cl-B = hollow clay bricks, AAC-B = aerated autoclaved blocks

At DS1, the increment of drift capacity appears to be systematic for each specimen with openings considering the "reference solid" test (see Table 12). At DS2, the ratio Ω varies between 0.90 (in some cases of infill panels with hollow clay bricks) and 1.78 (for panels with solid clay bricks). More variability of Ω can finally be observed at DS3 and DS4. Notably, data related to "concrete" in Table 12 are related to AAC-B only because no useful data are available for the NC-B panels with openings, which are the aim in this section.

In summary, the mean and CoV values of the Ω_i (i = 1,…,4) ratios are finally shown in Table 13, also depending on the infill material typology, as classified in Sect. 3.2. If

Table 13 Ω ratios at each DS depending on brick material

Ω		With openings/no openings				
		DS1	DS2	DS3	DS4	$\overline{\Omega}$
All	n_i	13	16	6	21	1.24
	Mean	1.31	1.18	1.26	1.23	
	CoV	0.33	0.20	0.49	0.39	
Clay (Cl-B)	n_i	11	16	4	17	1.16
	Mean	1.15	1.18	0.87	1.21	
	CoV	0.15	0.20	0.21	0.37	
Concrete (AAC-B)	n_i	2	0	2	4	1.72
	Mean	2.18	–	2.02	1.33	
	CoV	0.18	–	0.11	0.47	

Cl-B clay bricks, *AAC* aerated autoclaved blocks

all data are analysed together (see Table 13), notably, the presence of openings generally leads to an increment of drift capacity from + 18% (namely, Ω = 1.18, see DS2) to + 31% (namely, Ω = 1.31, see DS1) on average with respect to the corresponding tests without openings, with a CoV of 35%. As a result, the increment of drift capacity due to openings considering all DSs ($\overline{\Omega}$), weighted depending on the number of specimens for each DS, is equal to approximately +24% (namely, $\overline{\Omega}$ = 1.24). Such an increment is more evident for infills made up of concrete blocks (mean value of Ω ranges from 2.18 at DS1 to 1.33 at DS4), as shown in Table 13, which results in a smaller CoV (25% on average). In this case, the weighted mean $\overline{\Omega}$ is equal to 1.72. A lower influence of openings can be observed for infills with clay bricks, for which the $\overline{\Omega}$ coefficient is equal to 1.16 considering all the DSs (see Table 13). The only exception to the drift capacity increment due to openings is the DS3 for solid clay bricks, where only four data points are available.

The coefficient $\overline{\Omega}$ could be useful to modify fragility curves for infills with openings starting from the fragility curves presented in Sect. 3.3.1. In particular, it can be assumed that for all DSs the IDR capacity values of infills without openings can be multiplied by the same coefficient, $\overline{\Omega}$, to obtain the IDR capacity of the corresponding infills with openings. As a result, $\overline{\Omega}$ can be adopted as a multiplier of the median drift capacity (e^{μ}) of the fragility curves obtained above, with the same logarithmic standard deviation.

These results can be further analysed, focusing on infills made up of clay bricks, for which more data are available. The Ω ratios between the IDR capacity of each specimen with openings and its corresponding "reference solid" test are reported in Fig. 4a, b depending on the opening size (void-to-total infill area, A_{op}/A_w) and the opening eccentricity (as defined in Sect. 2, x/L_w). Only data related to DS3 are missing due to the very small number of available data. First, the Ω ratios are generally higher than or equal to the unity (in 100% of cases at DS1 and approximately 75% of cases at DS2 and DS4). Then, at DS1, Ω ratios remain nearly constant when A_{op}/A_w or x/L_w increases. A significant reduction in the Ω ratio can be observed at DS2 when the opening size increases. Finally, a very slight increment of Ω is observed at DS4 when A_{op}/A_w or x/L_w increases.

Furthermore, an analysis of the opening size and eccentricity effects on drift capacity by means of the experimental studies performed by Kakaletsis and Karayannis (2007, 2008, 2009) and Sigmund and Penava (2012) could be helpful. Such experimental studies explicitly compare the performance of infills without openings with the corresponding infills

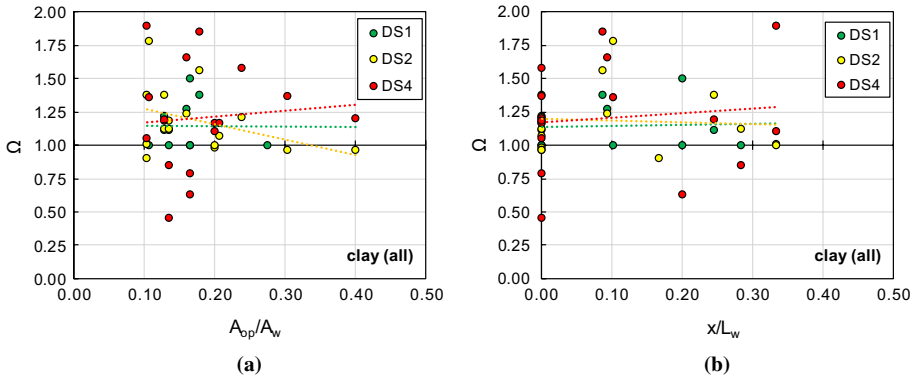

Fig. 4 Ω ratios depending on the opening ratio (**a**) and opening eccentricity (**b**)

with openings (different for void ratio and eccentricity). Tests WO2, WO4 and WO3 by Kakaletsis and Karayannis (2007, 2009) have the same eccentricity (concentric window) but different opening sizes (0.10 for test WO2; 0.21 for test WO4; 0.24 for test WO3). The presence of openings produces a drift capacity increment, which is constant on average with the opening size at DS2, whereas at DS4, the higher the opening size, the higher the drift capacity. On the other hand, if tests WO2, WX2, and WX1 by Kakaletsis and Karayannis (2007) are observed, notably, the void ratio is the same for all tests, whereas the opening eccentricity increases from WO2 to WX1. For these tests, analysing IDR_{DS2} confirms that an increment in drift capacity is generally observed due to the opening presence (eccentric or concentric), and a nearly constant trend can be identified between opening eccentricity and drift capacity. This conclusion is also confirmed by tests I/1, I/2, I/3, and I/4 by Sigmund and Penava (2012), which are different from each other only in terms of opening eccentricity.

In conclusion, based on the experimental data collected herein, a drift capacity increment of infills with openings is observed with respect to the corresponding "reference solid" panel, which is more evident for concrete blocks and less significant for clay bricks. However, further experimental studies are needed to perform a more comprehensive analysis of the effects of openings on drift capacity, also considering the opening size and its eccentricity.

4 DSs and in-plane response of infills

In the previous section, the drift capacity of infill panels was investigated by means of "observational" data for all DSs, without any consideration of the in-plane force, or drift response of the infill panel. However, it could be interesting to find the relationship between (i) the drift capacity at each DS and (ii) the drift corresponding to the peak load of the in-plane response of the infill panel (IDR_{peak}). Such a relationship can be used to derive information about drift capacity at each DS starting from the in-plane response of the panel only, for example.

With this aim, among all the collected tests, only infills without openings (79 tests) are considered, since these infills represent the major part of the collected database. Among these tests, in 24 cases, the authors of the experimental campaigns explicitly reported the

Table 14 IDR_{peak} and α_i ratios

	References	Label	IDR_{peak} (%)	α_1 (−)	α_2 (−)	α_3 (−)	α_4 (−)
H-Cl-B	Bergami and Nuti (2015)	Ft1	1.06	0.15	0.66	1.23	–
	Calvi and Bolognini (2001)	6	0.17	–	1.17	2.34	–
	Colangelo (2005)	V11	0.36	0.06	–	–	6.18
		V21	0.30	0.10	–	–	6.84
		V22	0.38	0.07	–	–	5.96
	Gazic and Sigmund (2016)	O3_bpm	0.34	0.45	0.96	–	2.80
		O4_bpm	0.26	0.70	1.11	–	3.64
	Guidi et al. (2013)	URM_U	0.81	0.12	–	–	–
	Kakaletsis and Karayannis (2008)	S	0.89	–	0.31	–	2.14
	Morandi et al. (2014)	TA2	0.77	0.39	0.65	2.28	3.26
	Sigmund and Penava (2012)	2/III	0.22	0.41	0.92	2.63	5.02
	Verderame et al. (2016)	GI-80	0.46	0.33	1.09	2.83	3.70
		SI-80	0.40	0.37	1.25	3.25	5.00
	Zovkic et al. (2013)	Model 4	0.13	0.15	–	–	–
		Model 8	0.11	0.18	–	–	–
	Waly (2010)	2	0.44	0.50	1.32	3.89	–
	Ricci et al. (2017)	IP + OOP_H	0.34	0.20	0.68	1.27	–
S-Cl-B	Gazic and Sigmund (2016)	O3_cpm	0.76	0.22	0.70	–	1.78
		O4_cpm	1.14	0.14	0.41	–	1.42
	Mansouri et al. (2014)	S	1.40	0.04	–	–	2.50
NC-B	Mehrabi et al. (1996)	4	0.43	–	0.40	2.32	–
		5	0.46	–	0.72	2.89	–
	Suzuki et al. (2017)	1S-1B	0.66	0.15	–	1.52	4.55
		1S-1B-V	0.42	–	–	3.57	7.14

S-Cl-B = solid clay bricks, H-Cl-B = hollow clay bricks, NC-B = normal concrete blocks

Table 15 Mean and CoV of α_i ratios

α_i	DS1			DS2			DS3			DS4		
	n_1	Mean	CoV	n_2	Mean	CoV	n_3	Mean	CoV	n_4	Mean	CoV
All (w/o openings)	19	0.25	0.71	15	0.82	0.39	12	2.50	0.34	15	4.13	0.45
Clay (Cl-B)	18	0.26	0.71	13	0.86	0.37	8	2.46	0.37	13	3.86	0.46
Hollow bricks (H-Cl-B)	15	0.28	0.67	11	0.92	0.34	8	2.46	0.37	10	4.45	0.35
Solid bricks (S-Cl-B)	3	0.13	0.71	2	0.55	0.37	0	–	–	3	1.90	0.29
Concrete (NC-B)	1	0.15	–	2	0.56	0.41	4	2.57	0.34	2	5.84	0.31

experimental responses of the tested infilled frames and the corresponding bare frames. Therefore, for these tests, it was possible to evaluate the experimental response of the infill panel.

First, the infill experimental response of each test, in terms of horizontal load-versus-horizontal drift, has been derived as the difference between the infilled frame and the corresponding bare frame (as explained in De Risi et al. 2018). Then, the relative position

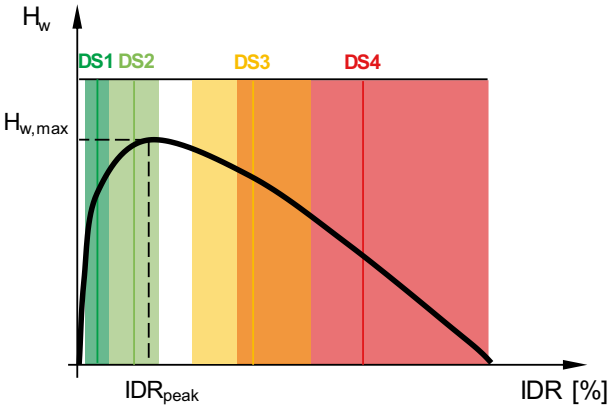

Fig. 5 DSs location on an ideal IDR-force relationship of infills; all data (w/o openings)

of each IDR_{DSi} (i = 1,…,4) with respect to the IDR_{peak} can be identified, as reported in Table 14. The IDR_{DSi} (i = 1,…,4)-to-IDR_{peak} ratio is hereinafter referred to as α_i (see Table 14). Table 15 shows the mean values and corresponding CoV for α_i ratios, both considering all test data together or separately depending on material and brick typology. Note that data related to "concrete" in Tables 14 and 15 are related to NC-B only because the in-plane response of AAC-B panels could not be evaluated.

When all data (w/o openings) are considered together, DS1 occurs at an IDR value (IDR_{DS1}) equal to 1/4·IDR_{peak}, on average (namely, $\alpha_i = 0.25$), whereas the IDR_{DS2} value is equal to approximately 80% of IDR_{peak} on average. Furthermore, the correspondence between the attainment of DS2 and peak load (namely, $\alpha_2 = 1$) has been assumed in the literature for hollow clay masonry infills, e.g., in Hak et al. (2012) and Ricci et al. (2013, 2016), assuming a correspondence between DS2 and DL PL, see Sect. 3.1, or Sassun et al. (2016). Based on data collected and analysed herein, this assumption can be confirmed for hollow clay bricks ($\alpha_2 = 0.92$). However, such a correspondence cannot be applied if only infills with solid bricks or concrete blocks are considered (see Table 15), as in these cases, DS2 is achieved for an IDR value, which is approximately one half of IDR_{peak} on average. Nevertheless, very few data (see Table 15) are available for these two infill types, and therefore, more data should support this outcome in future works.

For DS3 and DS4, the values of α_3 and α_4 are equal to approximately 2.50 and 4.10, respectively. The result at DS4 appears to agree with Dolšek and Fajfar (2008), according to which the drift at collapse is assumed to be equal to 5 times the peak load drift.

Finally, high CoV values of α_i are confirmed at less severe DSs, especially at DS1.

Starting from the values of α_i shown in Table 15, Fig. 5 graphically shows the DSs boundaries on a typical IDR-force (H_w) relationship of an infill panel (considering "All" data without openings). $H_{w,max}$ in Fig. 5 represents the lateral strength of the infill. For each DS, the mean values of α_i (i = 1,…,4) are reported with solid lines, and DSs boundaries (shadowed areas) are defined by the 16th and 84th percentiles of α_i.

5 Loss estimation

In previous sections, fragility curves in terms of IDR values have been defined, considering the influence of brick materials and opening typologies. Hereinafter, the loss function term is derived for the same infill typologies, thus providing expected monetary loss conditioned to the attainment of a given damage state and on the attainment of a given IDR threshold.

To this end, a list of macroactivities has to be fixed, determining the main operations in repairing an infill panel damaged during a seismic event, which is as follows:

(a) *Preliminary operations* preparatory activities for regular construction, namely, installation of scaffolding and enclosure;
(b) *Demolition* activities connected to the demolition of plaster, single brick units or the entire panel (if necessary and depending on the damage level);
(c) *Reconstruction* activities connected with infill panel restoration, namely, the execution of single brick units or the entire panel (if necessary and depending on the damage level);
(d) *Finishing* activities connected to the execution of plastering/rendering layers, painting and coating operations;
(e) *Windows* activities connected to the disassembling of old window/door frames (if present) and the installation of new or old window/door frames;
(f) *Landfill* activities connected to transportation and disposal of waste produced during the demolition/repair activities; and
(g) *Technical cost* design and construction management activities.

Then, each activity group, from *a* to *g*, is made of a list of elementary actions, established based on engineering judgement to restore the infill panel to its undamaged state, as reported in Table 16, in which the corresponding unit cost, (c_j), was evaluated using the Price List of Public Works in Abruzzi Region (B.U.R.A. 2017). Furthermore, nearly all elementary actions can be performed using different technologies and materials, and, consequently, different unit costs can be found in the assumed price list. In fact, scaffolding installation can be performed using standard, putlog and ledgers, steel prefabricated frames or multidirectional ring-lock rosettes. Demolition of a single leaf masonry panel has a different cost, according to the assumed price list, as a function of brick typology and to the adopted execution procedure (handmade or with mechanical equipment). Rendering layer and painting has a different cost as a function of the material used. Installation of a new window has a different cost as a function of the material typology used for the frame and the thickness of glazing and of the interposed cavity. Thus, Table 16 reports the elementary actions assumed in the present work and their corresponding unit costs.

Technical costs, including fees for structural engineers, project engineers, and construction managers, are assumed to be equal to 8% of the total cost of the intervention (as suggested by Cardone and Perrone 2015).

Notably, each elementary action affects different areas of the infill panel ($A_{j,DSi}$) as a function of the assumed damage pattern, i.e. as a function of the achieved DS_i ($i=1,\ldots,4$). Obviously, the definition of the ($A_{j,DSi}$) term follows the damage extension (detachment, cracking, failure of brick units), which is assumed in Sect. 3.1 and reported in Table 16. In fact, *demolition and plastering activities* affect a strip width of 0.20 m across each diagonal (d), where cracks occur, and for each side at DS1, 30% of the entire panel area for each side

Table 16 Unit cost and extension of repair areas for assumed elementary actions according to the price list for Public Works in the Abruzzi region, Italy (2016)

Activity group	Elementary actions	Unit	Unit cost (c_j)	$AA_{j,DS1}$	$A_{j,DS2}$	$A_{j,DS3}$	$A_{j,DS4}$
(a) Preliminary operations	Install scaffolding with steel scaffolding and multidirectional ring-lock rosettes, with fibreglass monofilament netting for scaffolding enclosure	€/mq	25.72	$(H_w \times L_w)$	$(H_w \times L_w)$	$(H_w \times L_w)$	$(H_w \times L_w)$
(b) Demolition activities	1. Demolition of single leaf masonry brick with mechanical equipment	€/mq	13.84	–	$10\%(H_w \times L_w)$	$(H_w \times L_w)$	$(H_w \times L_w)$
	2. Render or plaster removal up to 5 cm thick (including surface brushing of affected area)	€/mq	8.58	$(0.20\ m) \times d$	$30\%(H_w \times L_w)$	$(H_w \times L_w)$	$(H_w \times L_w)$
(c) Construction activities	1. Construction of infill panels:			–	$10\%(H_w \times L_w)$	$(H_w \times L_w)$	$(H_w \times L_w)$
	i. Construction of single leaf masonry wall using concrete bricks (300 mm thick)	€/mq	47.82				
	ii. Construction of double leaf cavity masonry wall (25 × 12 × 5,5 solid clay brick for exterior leaf and 12,5 × 25 × 25 hollow clay brick for interior leaf)	€/mq	78.95				
	iii. Construction of double leaf cavity masonry wall (25 × 12 × 5,5 semisolid clay brick for exterior leaf and 12,5x25x25 hollow clay brick for interior leaf)	€/mq	116.70				
	iv. Construction of double leaf cavity masonry wall (12 × 25 × 25 hollow clay brick for exterior leaf and 8 × 25 × 25 hollow clay brick for interior leaf)	€/mq	72.58				
	2. Cavity thermal insulation with glass mineral wool	€/mq	22.78				
(d) Finishings	1. Coat rendering or plastering (3 layers) with cement mortar	€/mq	23.86	$(0.20\ m) \times d$	$(30+10)\%$ $(H_w \times L_w)$	$(H_w \times L_w)$	$(H_w \times L_w)$
	2. Water-based primer application	€/mq	2.53	$(H_w \times L_w)$	$(H_w \times L_w)$	$(H_w \times L_w)$	$(H_w \times L_w)$
	3. Coating painting (3 layers) for each side with water-based paint	€/mq	13.19	$(H_w \times L_w)$	$(H_w \times L_w)$	$(H_w \times L_w)$	$(H_w \times L_w)$

Table 16 (continued)

Activity group	Elementary actions	Unit	Unit cost (c_j)	$AA_{j,DS1}$	$A_{j,DS2}$	$A_{j,DS3}$	$A_{j,DS4}$
(e) Window or door frame installation	1. Installation of new or old window or door opening						
	i. Installation of new window or door opening with solid wood frame with Douglas fir trees, double insulation glazing 5 mm thick with argon gas cavity (12 mm thick), wooden box shutter (Douglas fir tree) and PVC rolling shutter	€/mq	542.64	–	–	–	$(H_{op} \times L_{op})$
	ii. Installation of old window or door opening with solid wood frame, glazing and rolling shutter (manpower only)	€/mq	62.36	–	–	$(H_{op} \times L_{op})^{**}$	–
	2. Removal of solid wood frame, box and roller shutter	€/mq	34.12	–	–	$(H_{op} \times L_{op})^{**}$	$(H_{op} \times L_{op})^{**}$
(f) Landfill	1. Landfill transportation	€/mc	26.24	(0.20 m) × d × (0.10 m)	(30) %$(H_w \times L_w)$ × (0.10 m) + (10) %$(H_w \times L_w)$ × $(t_w + 0.10\ m)$	$(H_w \times L_w)$ × $(t_w + 0.10\ m)$	$(H_w \times L_w)$ × $t_w + 0.10\ m)$
	2. Landfill disposal*	€/t	15.18*				
(g) Technical cost	Technical cost	%	8.00	$\sum_{j}^{\{a,b,c,d,e,f\}} c_j A_{j,DS1}$	$\sum_{j}^{\{a,b,c,d,e,f\}} c_j A_{j,DS2}$	$\sum_{j}^{\{a,b,c,d,e,f\}} c_j A_{j,DS3}$	$\sum_{j}^{\{a,b,c,d,e,f\}} c_j A_{j,DS4}$

*Published in Update of the Regional Price List for Reconstruction after the April 6, 2009 earthquake B.U.R.A. (2009)

**"H_{op}" and "L_{op}" are the height and length of the opening, respectively

at DS2, and the entire area for each side at DS3 and DS4. *Construction activities* affect 10% of the panel area at DS2, and 100% of the panel areas at DS3 and DS4. For simplicity, $A_{j,DS1}$ for activities connected to plaster removal, restoration and landfill disposal is computed for panels with window or door openings as (0.20 m × d), thus producing a slight overestimation in loss estimation due to computing the above activities on a small portion (the intersection between $A_{j,DS1}$ and opening area) actually occupied by the opening.

On the other hand, *preliminary and painting activities* are performed on the entire infill panel area ($H_w \times L_w$). Existing *window and door openings* (if any) are removed and reinstalled at DS3, whereas a new unit (wood frame with insulated glazing, wooden box shutter, PVC shutter) is installed at DS4. The volume and weight of waste are evaluated considering the quantities produced during all demolition activities.

Then, summarizing the product of the cost (c_j) and the area of intervention ($A_{j,DSi}$) for all activity groups in Table 16, the total restoration cost of an infill panel damaged during a seismic event for a given damage state (DS_i) can be evaluated as follows:

$$C_{DSi}^{TOT} = \sum_{j}^{\{a,b,c,d,e,f,g\}} c_j A_{j,DSi}$$

Similarly, considering only *b–e* activities, the cost of "demolition and repair/construction" of a damaged infill panel can be evaluated as follows:

$$C_{DSi}^{Dem\&Const} = \sum_{j}^{\{b,c,d,e\}} c_j A_{j,DSi}$$

Finally, considering only the ancillary actions, regarding *a, f* and *g* activities, the cost of activities "complementary" to the cost of demolition and reconstruction of a damaged infill panel can be evaluated as follows:

$$C_{DSi}^{Compl} = \sum_{j}^{\{a,f,g\}} c_j A_{j,DSi} = C_{DSi}^{TOT} - C_{DSi}^{Dem\ \&\ Const}$$

hence C_{DSi}^{TOT} for three (solid, with window and door opening) panel typologies is herein evaluated, following a Monte Carlo simulation technique, which considers a number of N = 1000 realizations varying with the length dimension of the infill panel, L_w, from 4.00 m to 5.00 m and assuming the height is equal to $H_w = 2.75$ m.

It is assumed herein that the clay infill panel can be realized using a double leaf cavity masonry wall with the following attributes:

- (*Solid + hollow*) *panel,* constituted by (12 × 25 × 5.5) cm solid clay brick for exterior leaf and (12.5 × 25 × 25) cm hollow clay brick (void percentage > 55%) for interior leaf with thermal insulation;
- (*Semisolid + hollow*) *panel,* constituted by (12.5 × 25 × 5.5) cm semisolid clay brick (0 ≤ void percentage ≤ 55%) for exterior leaf and (12.5 × 25 × 25) cm hollow clay brick (void percentage > 55%) for interior leaf with thermal insulation;
- (*Hollow + hollow*) *panel,* constituted by (12 × 25 × 25) cm hollow clay brick (void percentage > 55%) for exterior leaf and (8 × 25 × 25) cm hollow clay brick (void percentage > 55%) for interior leaf with thermal insulation;

Table 17 Repair costs (C_{DS4}^{TOT}) considering different brick materials and infill typologies

	C_{DS1}^{TOT} (€/m^2)	C_{DS2}^{TOT} (€/m^2)	C_{DS3}^{TOT} (€/m^2)	C_{DS4}^{TOT} (€/m^2)
(*Hollow* + *hollow*) *clay*				
Solid panel	77.0	105.3	285.8	285.8
Panel with window	73.0	101.3	270.1	331.4
Panel with door	69.2	97.4	255.2	374.9
(*Hollow* + *semisolid*) *clay*				
Solid panel	77.0	110.0	333.5	333.5
Panel with window	73.0	106.0	312.2	373.4
Panel with door	69.2	102.2	291.8	411.5
(*Hollow* + *solid*) *clay*				
Solid panel	77.0	106.0	292.7	292.7
Panel with window	73.0	102.0	276.2	337.4
Panel with door	69.2	98.1	260.5	380.2
Concrete				
Solid panel	77.0	102.6	259.1	259.1
Panel with window	73.0	98.6	246.6	307.8
Panel with door	69.2	94.8	234.6	354.3

and for the *concrete panel,* a single leaf masonry wall 300 mm thick is considered.

Openings are assumed to be composed of wood frames with plan dimensions of (1.20 × 2.20) m^2 or (0.90 × 1.50) m^2 for a door or window opening, respectively.

C_{DS4}^{TOT} for each panel typology at DS_i (i = 1,…,4) are reported in Table 17 (in euros (€) per square metre of panel). As seen in Table 17, in the case of solid panels, the total repair cost for DS3 and DS4 is exactly the same, since all the unit costs (c_j) and areas of intervention ($A_{j,DSi}$) have exactly the same value, as reported in Table 16.

Notably, the total cost at DS3, C_{DS3}^{TOT}, is evaluated considering the replacement of the entire panel area (namely, in Table 16, $A_{j,DS3} = H_w \times L_w$), i.e., assuming that at this DS, the repair cost is unreasonable compared to the replacement cost, whereas in Sect. 3.1, it is reported that the area affected by a wide spreading of crushing and spalling of brick units at DS3 is up to 30% of the panel area. In the hypothesis of considering an $A_{j,DS3} = 0.30(H_w \times L_w)$, according to the damaged area reported in Sect. 3.1, the total cost at DS3 is equal to 55% of the total replacement cost on average. Thus, according to the FEMA P-58 (2012b) recommendation, the infill panel is likely to be replaced rather than repaired, with the corresponding repairing cost being greater than the assumed threshold equal to 50% of C_{DS4}^{TOT}. Therefore, DS3 is herein assumed to be the damage level in which the infill panel is *not repairable at reasonable cost*, justifying the assumption made in Table 16 regarding $A_{j.DS3}$.

The ratios $\chi_{DSi} = C_{DSi}^{TOT}/C_{DSi}^{Dem\&Const} = (1 + C_{DSi}^{Compl}/C_{DSi}^{Dem\ \&Const})$ (with i = 1,…,4) are herein evaluated for each DS and for each panel typology. Obviously, χ_{DSi} values decrease with increasing severity of damage (from DS1 to DS4), since the contribution of "complementary" activities (***a***, ***f*** and ***g***),C_{DSi}^{Compl}, decrease compared to $C_{DSi}^{Dem\ \&\ Const}$.

For example, for (hollow + hollow) clay infill panel typology, χ_{DSi} values range between 1.78 (at DS1) and 1.33 (at DS4) for a solid panel, between 1.85 (at DS1) and 1.28 (at DS4) for a window opening-panel, and between 1.93 (at DS1) and 1.25 (at DS4) for a door opening-panel.

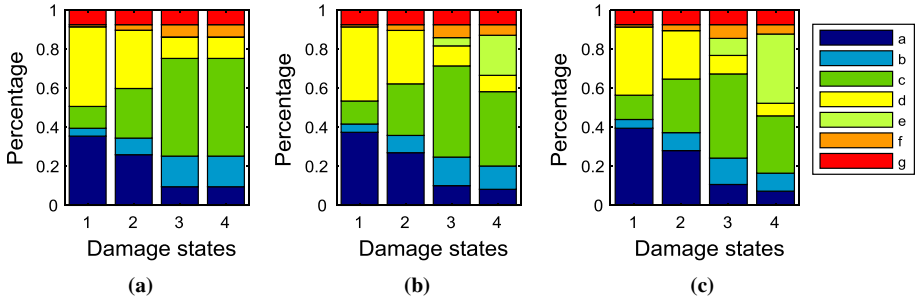

Fig. 6 Contribution of considered activities on total repair cost for (hollow + hollow) clay brick panels (without (**a**) and with window (**b**) and door (**c**) openings

Such trends can be better analysed, considering the de-aggregation of C_{DSi}^{TOT} for each considered elementary action, showing its contribution to a given damage level. For simplicity, Fig. 6 reports the de-aggregation of C_{DSi}^{TOT} for only a double leaf cavity masonry wall, (hollow + hollow) clay panel with different opening configurations. The following can be noted:

- *a* and *d* activities represent approximately 75% of C_{DS1}^{TOT}, disregarding opening configurations, and only 17% of C_{DS4}^{TOT}. The decreasing percentage weights can be explained by the fact that the corresponding $A_{j,DSi}$ terms remain invariant with DS_i while C_{DSi}^{TOT} increases;
- Conversely, *b*, *c* and *e* (if any) activities represent approximately 16% of C_{DS1}^{TOT} and approximately 70% of C_{DS4}^{TOT}. The increasing trend can be explained by the corresponding $A_{j,DSi}$ terms increasing with damage severity.

The values in Table 17 are considered to be expected (mean) values of economic losses for restoring a damaged infill partition after an earthquake. A dispersion value around them may be considered due to variability related to different professional practises, different unit costs in different geographical areas or considering uncertainty in contractor pricing strategies. Hence, expected values of economic losses together with fragility curves for different infill panel typologies and opening configurations are used to determine a *Direct Loss Analysis* function, L(IDR), providing a direct relationship between the probability of experiencing a certain level of monetary loss conditioned on the attainment of a given IDR request in the infill panel:

$$L(IDR) = \sum_i \sum_j P\left[DS_i|IDR\right] \cdot c_j \cdot A_{j,DSi} = \sum_i P\left[DS_i|IDR\right] \cdot C_{DSi}^{TOT} \tag{3}$$

The term C_{DSi}^{TOT} is determined considering the values for each infill panel typology reported in Table 17, while $P\left[DS_i|IDR\right]$ represents the probability of occurrence of the i^{th} DS as a function of IDR. This probability is evaluated by means of the lognormal fragility curves, $\Phi_{DSi}(\bullet)$, reported in Sect. 3, as in Eq. (4) for i = 1,…,3:

$$P\left[DS_i|IDR\right] = \Phi_{DSi}(\cdot) - \Phi_{DSi+1}(\cdot) = \Phi\left(\frac{\ln(IDR) - \mu_i}{\beta_i}\right) - \Phi\left(\frac{\ln(IDR) - \mu_{i+1}}{\beta_{i+1}}\right) \tag{4}$$

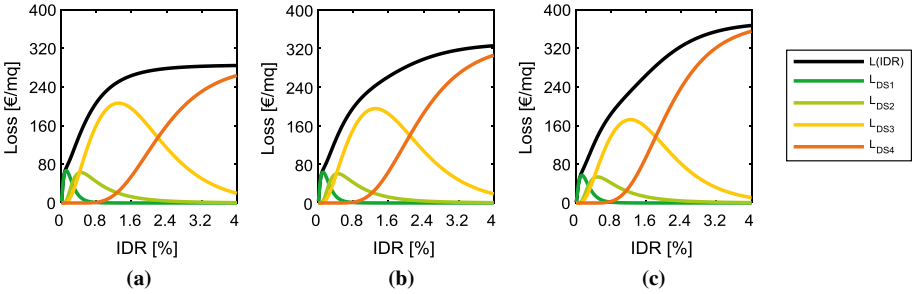

Fig. 7 L(IDR) function for (hollow + hollow) clay panels: without (**a**) and with window (**b**) and door openings (**c**)

otherwise $P[DS_4|IDR] = \Phi_{DS4}(\cdot)$.

Therefore, for clay and concrete brick typologies, $P[DS_i|IDR]$ terms are evaluated considering the fragility curves in Table 10 and Table 11. In particular:

- For (hollow + hollow) and (semisolid + hollow) clay infill panel typology, the $P[DS_i|IDR]$ term is determined considering fragility curves for hollow clay bricks; in particular, being that $H_w\backslash t_w = 22.9$ for the analysed case study, the fragility curves for slender infills ($H_w\backslash t_w > 12$) will be used hereinafter;
- For (solid + hollow) clay infill panel typology, the $P[DS_i|IDR]$ term is determined considering both fragility curves for hollow and solid clay bricks; to reproduce the behaviour of both layers conservatively, the maximum value of exceeding probability given the IDR value has been considered between the two abovementioned fragility curves for slender infills;
- For concrete infill panel typology, the $P[DS_i|IDR]$ term is determined considering fragility curves for concrete blocks.

Finally, fragility curves for different opening configurations are evaluated from those of the panel typologies without openings, which is multiplied by the related $\overline{\Omega}$ coefficient (reported in Table 13).

Figure 7 reports the conceptual derivation of the L(IDR) function for the (hollow + hollow) panel, obtained by summarizing each DS_i contribution, $P[DS_i|IDR] \cdot C_{DSi}^{TOT}$. Notably, the L(IDR) function tends toward C_{DS4}^{TOT} for high IDR values.

Figure 8 shows the influence of brick typologies on the L(IDR) function derivation for different opening typologies. For very low IDR values, the curves exactly overlap, with the resulting costs dominated by activities *a* and *d*, which have the same unit cost, when disregarding brick typologies. The curves tend to diverge when the influences of *b*, *c* and *e* (if any) activities become more significant on the repair cost, namely, starting from 0.5% IDR values. Furthermore, L(IDR) function related to (hollow + hollow) and (solid + hollow) clay panels are quite similar, since (i) these panels have similar C_{DSi}^{TOT} (see Table 17), and (ii) the $P[DS_i|IDR]$ term has been determined considering the maximum value of exceeding probability between both fragility curves for hollow and solid clay bricks.

Figure 9 shows the influence of different opening typologies on the L(IDR) function derivation for brick typologies. Notably, there is a negligible influence of the opening typology up to IDR = 1.5%, being C_{DSi}^{TOT} (for i = 1,…,3) similar for each brick typology (see

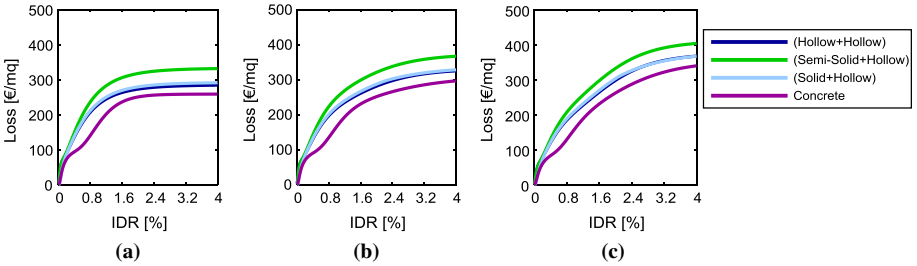

Fig. 8 L(IDR) function for hollow clay panels [without (**a**) and with window (**b**) and door openings (**c**)]

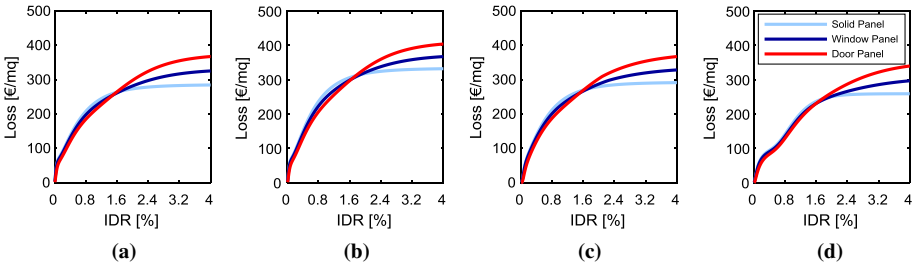

Fig. 9 L(IDR) function for (hollow + hollow) (**a**), (semisolid + hollow) (**b**), (solid + hollow) (**c**), and concrete (**d**) panels

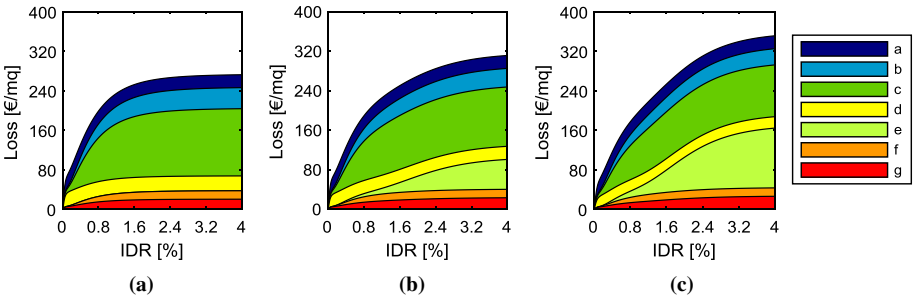

Fig. 10 L(IDR) function for each activity group for (hollow + hollow) panels [without (**a**) and with window (**b**) and door openings (**c**)]

Table 17). Such differences are produced by $A_{j,DSi}$ values for panels with openings, which have to be adjusted to account for the area of the opening, leading to slightly lower C_{DSi}^{TOT} values with respect to solid panels (see Table 17). For higher IDR values (> 1.5%), the opening replacement cost counterbalances this trend, leading to significantly higher C_{DSi}^{TOT} values with respect to solid panels.

Figure 10 shows the de-aggregation of the L(IDR) function for each elementary action considered, showing its contribution as a function of IDR for hollow clay bricks with different opening configurations. Obviously, for very low IDR values, the elementary activities, namely, *a* and *d* activities, which play a significant role in the definition of less severe damage levels (i.e., C_{DS1}^{TOT}), have a greater influence on the definition of the L(IDR)

Table 18 Nonlinear regression coefficients for the definition of the $\bar{L}(IDR)$ function

	γ	C^{Const} (€/m^2)	b_1	b_2
(*Hollow* + *hollow*) *clay*				
Solid panel	1.64	174.52	1.61	0.91
Panel with window	1.52	217.96	1.09	0.84
Panel with door	1.44	259.48	0.84	0.97
(*Hollow* + *semisolid*) *clay*				
Solid panel	1.53	218.64	1.54	0.97
Panel with window	1.45	256.88	1.09	0.88
Panel with door	1.40	293.41	0.86	0.99
(*Hollow* + *solid*) *clay*				
Solid panel	1.62	180.89	1.60	0.97
Panel with window	1.51	223.58	1.07	0.85
Panel with door	1.44	264.38	0.83	0.96
Concrete				
Solid panel	1.73	149.76	1.23	1.19
Panel with window	1.57	196.13	0.82	1.01
Panel with door	1.47	240.43	0.63	1.13

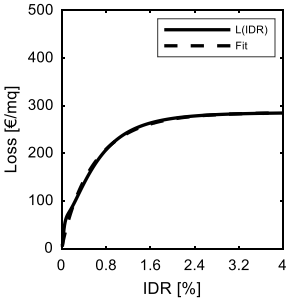

As an example, a comparison is shown between the rigorous L(IDR) function and fitted $\bar{L}(IDR)$ function for (hollow + hollow) solid panel

function. Conversely, for high IDR values, the elementary activities, namely, activities *b*, *c* and *e* (if any), which play a significant role in the definition of more severe damage levels (i.e., C_{DS4}^{TOT}), have a greater influence on the definition of the L(IDR) function.

Finally, in the hypothesis considering a slightly different C_{DS4}^{TOT} value, attempting to find a variation in unit cost or for the introduction of a different elementary action (for example, wooden louver instead of PVC rolling shutter), an extension of this approach is considered in a very simplified manner. As previously highlighted, the repair cost C_{DS4}^{TOT} is evaluated considering all the elementary actions listed in Table 16. Thus, a slight variation in a single elementary action also leads to a complex calculation to update all the $c_j A_{j,DS4}$ values. On the other hand, the cost of "construction of a new infill panel" (C^{Const}) can be evaluated considering a very limited number of elementary actions (only ***c*** to ***e*** activities); moreover, C^{Const} could be assumed as a portion (expressed herein as $1/\gamma$) of the total repair cost C_{DS4}^{TOT}. In such a way, the substitution of the term ($C_{DS4}^{TOT} = \gamma \cdot C^{Const}$) would significantly simplify the presented loss estimation procedure to account for slight variations in unit costs. This is rigorously true if no other terms vary except for the *c*, *d* and *e* unit costs, leading to the same γ value. Otherwise, the γ value evaluated in Table 18 would change according to the assumed variations in unit costs.

Then, for a simplified practice-oriented loss estimation approach, it may be assumed in any cases that the γ values of Table 18 only vary (if necessary) based on the C^{Const} term, disregarding any changes in the remaining terms. Table 18 reports the estimated b_1 and b_2 nonlinear regression coefficients, considering the functional form $\bar{L}(IDR) = C_{DS4}{}^{TOT} \cdot [1 - \exp(-b1 \cdot IDR^{b2})]$, together with the C^{Const} and γ values, whereas the C_{DS4}^{TOT} values are reported in Table 17.

6 Conclusions

In the present work, damage and loss analyses for masonry infills with clay or concrete bricks in RC frames were investigated. To this end, an experimental database for this infill typology on one-bay, one-story scaled RC frames was collected, presented and analysed. For these tests, the drift capacity at each performance level was identified starting from the description of the damage evolution under increasing drift demand. ECD functions have been obtained, and lognormal fragility functions have been adopted to fit the data.

The collected database was divided into homogeneous data subsets, thus obtaining drift-based fragility curves that explicitly depend on infill brick materials and their main geometrical and mechanical properties. Therefore, more specific curves were derived for further applications, such as a more refined analysis of losses due to earthquakes for infilled RC buildings depending on the infill characteristics. Infills with concrete blocks exhibit a higher median drift capacity with respect to the corresponding values related to infills with clay bricks. Generally, a smaller drift capacity characterizes infills with solid clay bricks with respect to infills with hollow clay bricks at higher DSs. At the *Moderate Damage Level* (DS2), fragility curves related to different brick materials are very close to one another. Infills with aerated autoclaved concrete blocks generally show higher drift capacity with respect to normal concrete blocks.

For clay bricks infills, the slenderness ratio and the frame-to-infill relative strength ratio affect the drift capacity. In particular, from DS1 to DS3, the lower the slenderness ratio, the higher the drift capacity. Similarly, lower values of the frame-to-infill relative strength ratio lead to a higher drift capacity of the infill panel.

The drift capacity threshold at each DS was also correlated to the peak load point of the in-plane response of the infill panels to directly quantify the relationship that exists among them. Based on the data collected herein, the *Slight Damage Level* (DS1) occurs at a drift value equal to 1/4 of the drift at the in-plane peak load of the infill panel on average. DS2 is approximately coincident with the peak load IDR for hollow clay bricks; however, such a correspondence cannot be applied if only infills with solid bricks or concrete blocks are considered. *Severe Damage* (DS3) and *Collapse* (DS4) occur for drift values equal to approximately 2.50 and 4.10 times the drift at the in-plane peak load of the infill panel, respectively.

The influence of openings on drift capacities has also been considered through the analysis of experimental studies that tested both infilled frames with openings and related frames infilled with a solid panel, which are used as references. Based on the collected data, the presence of openings generally leads to a drift capacity increment, which is clearer for infills with concrete blocks. A lower influence of openings was observed for infills with clay bricks. Thus, some modification factors of infill fragility curves without openings have been proposed to obtain fragility curves for infills with openings.

Notably, due to the empirical nature of the obtained drift capacity, the conclusions drawn in this work are strictly related to the data collected herein and specifically to the variability ranges of mechanical properties (e.g., infill compressive strength, infill-to-frame relative strength and stiffness) and geometrical properties (e.g., infill aspect ratio, opening size and eccentricity, scale factor) of the collected specimens. Therefore, strictly speaking, these variability ranges should also represent the applicability thresholds of this work. A further effort should be performed in future works to enlarge the collected experimental database. In such a way, a further comprehensive clustering of data could be completed to investigate (i) the effects of all the geometrical and mechanical properties that can affect the in-plane response, (ii) the presence of openings (also considering the effects of opening size and its eccentricity), and (iii) the size effect on the evaluation of drift capacity thresholds.

Finally, seismic losses related to infills have been computed, which in this case also depend on the infill typology. All required repairing activities and their costs have been presented together with their incidence at each DS and explicitly evaluated as a function of drift demand. Loss functions directly depending on IDR demand have finally been provided in a closed (fitted) form for all investigated infill typologies, thus fusing together damage and loss analyses for a simpler, practice-oriented loss calculation.

Acknowledgements This work was developed under the support of ReLUIS-DPC 2014-2018 "*PR2. Strutture in cemento armato-WP6. Capacità sismica di tamponature ed interventi di rafforzamento"*, funded by the Italian Department of Civil Protection (DPC), and AXA Research Fund Post-Doctoral Grant "*Advanced nonlinear modelling and performance assessment of masonry infills in RC buildings under seismic loads: the way forward to design or retrofitting strategies and reduction of losses*". These financial supports are gratefully acknowledged.

References

Akhound F, Vasconcelos G, Lourenço PB, Palha CAOF, Silva LC (2015) In-plane and out-of plane experimental characterization of RC masonry infilled frames. In: M2D-6th international conference on mechanics and materials in design, pp 427–440

Alwashali H, Torihata Y, Jin K, Maeda M (2018) Experimental observations on the in-plane behaviour of masonry wall infilled RC frames; focusing on deformation limits and backbone curve. Bull Earthq Eng 16(3):1373–1397

Angel RD, Abrams DP, Shapiro D, Uzarski J, Webster M (1994) Behavior of reinforced concrete frames with masonry infills. University of Illinois Engineering Experiment Station. College of Engineering. University of Illinois at Urbana-Champaign

ASCE (2013) ASCE/SEI 41-13. Seismic evaluation and retrofit of existing buildings. American Society of Civil Engineers, Reston

Baggio C, Bernardini A, Colozza R, Coppari S, Corazza L, Della Bella M, Di Pasquale G, Dolce M, Goretti A, Martinelli A, Orsini G, Papa F, Zuccaro G (2007) Field manual for post-earthquake damage and safety assessment and short term countermeasures. Translation from Italian: Goretti A, Rota M, JRC Scientific and Technical Reports, EUR 22868 EN-2007

Baran M, Sevil T (2010) Analytical and experimental studies on infilled RC frames. Int J Phys Sci 5(13):1981–1998

Bergami AV, Nuti C (2015) Experimental tests and global modeling of masonry infilled frames. Earthq Struct 9(2):281–303

Bertoldi SH, Decanini LD, Gavarini C (1993) Telai tamponati soggetti ad azioni sismiche, un modello semplificato: confronto sperimentale e numerico. Atti del 6 Convegno Nazionale L'ingegneria sismica in Italia, pp 815–824

B.U.R.A. (Official Journal of Regione Abruzzo) (n. 10—08/03/2017—ordinary), Price List of Public Works in Abruzzi Region, Italy **(in Italian)**

B.U.R.A. (Official Journal of Regione Abruzzo) (n. 10—28/10/2009—extraordinary), Updating of the regional price list for reconstruction after the April 6, 2009 earthquake **(in Italian)**

Calvi GM, Bolognini D (2001) Seismic response of reinforced concrete frames infilled with weakly reinforced masonry panels. J Earthq Eng 5(02):153–185

Cardone D, Perrone G (2015) Developing fragility curves and loss functions for masonry infill walls. Earthq Struct 9(1):257–279

Cavaleri L, Di Trapani F (2014) Cyclic response of masonry infilled RC frames: experimental results and simplified modeling. Soil Dyn Earthq Eng 65:224–242

CEN (2005) Eurocode 8: design of structures for earthquake resistance-part 1: general rules, seismic actions and rules for buildings. European Committee for Standardization, Brussels

Centeno J, Ventura CE, Foo S (2008) Shake table testing of gravity load designed reinforced concrete frames with unreinforced masonry infill walls. In: The 14th world conference on earthquake engineering, Beijing

Chiou TC, Hwang SJ (2015) Tests on cyclic behavior of reinforced concrete frames with brick infill. Earthq Eng Struct Dyn 44(12):1939–1958

Chiozzi A, Miranda E (2017) Fragility functions for masonry infill walls with in-plane loading. Earthq Eng Struct Dyn 46(15):2831–2850

Chrysostomou CZ, Asteris PG (2012) On the in-plane properties and capacities of infilled frames. Eng Struct 41:385–402

Colangelo F (2005) Pseudo-dynamic seismic response of reinforced concrete frames infilled with non-structural brick masonry. Earthq Eng Struct Dyn 2005(34):1219–1241

Colangelo F (2013) Drift-sensitive non-structural damage to masonry-infilled reinforced concrete frames designed to Eurocode 8. Bull Earthq Eng 11(6):2151–2176

Crisafulli FJ (1997) Seismic behaviour of reinforced concrete structures with masonry infills. PhD Thesis, University of Canterbury

De Risi MT, Del Gaudio C, Ricci P, Verderame GM (2017). Simplified numerical modelling for hollow clay-masonry infills in RC frames under in-plane seismic loads. In: ANIDIS 2017, Pistoia

De Risi MT, Del Gaudio C, Ricci P, Verderame GM (2018) In-plane behaviour and damage assessment of masonry infills with hollow clay bricks in RC frames. Eng Struct 168:257–275

Decreto Ministeriale del (2008) Approvazione delle nuove norme tecniche per le costruzioni. G.U. n. 29 del 4/2/2008 **(in Italian)**

Del Gaudio C, Ricci P, Verderame GM, Manfredi G (2016a) Observed and predicted earthquake damage scenarios: the case study of Pettino (L'Aquila) after the 6th April 2009 event. Bull Earthq Eng 14(10):2643–2678

Del Gaudio C, De Martino G, Di Ludovico M, Manfredi G, Prota A, Ricci P, Verderame GM (2016b) Empirical fragility curves from damage data on RC buildings after the 2009 L'Aquila earthquake. Bull Earthq Eng. https://doi.org/10.1007/s10518-016-0026-1

Del Gaudio C, De Risi MT, Ricci P, Verderame GM (2017) Fragility functions for clay masonry infills in RC buildings under in-plane seismic actions. In: ANIDIS 2017, Pistoia

Dolce M, Goretti A (2015) Building damage assessment after the 2009 Abruzzi earthquake. Bull Earthq Eng 13(8):2241–2264

Dolšek M, Fajfar P (2008) The effect of masonry infills on the seismic response of a four-storey reinforced concrete frame—a deterministic assessment. Eng Struct 30(7):1991–2001

FEMA P-58, ATC—Applied Technology Council (2012b), FEMA P-58 Next-generation Seismic Performance Assessment for Buildings, vol 2—Implementation Guide, Federal Emergency Management Agency, Washington, DC

Frumento S, Magenes G, Morandi P, Calvi GM (2009). Interpretation of experimental shear tests on clay brick masonry walls and evaluation of q-factors for seismic design. Research Report EUCENTRE 2009/02, IUSS Press, Pavia, ISBN: 978-88-6198-034-1

Gazić G, Sigmund V (2016) Cyclic testing of single-span weak frames with masonry infill. Građevinar 68(08):617–633

Grünthal G., (1998). Cahiers du Centre Européen de Géodynamique et de Séismologie: vol 15—European macroseismic scale 1998. European Center for Geodynamics and Seismology, Luxembourg

Guidi G, da-Porto F, Dalla-Benetta M, Verlato N, Modena C (2013) Comportamento sperimentale nel piano e fuori piano di tamponamenti in muratura armata e rinforzata. Dipartimento di Ingegneria Civile, Edile e Ambientale, Padova

Haider S (1995) In-plane cyclic response of reinforced concrete frames with unreinforced masonry infills. PhD Thesis, Rice University

Hak S, Morandi P, Magenes G, Sullivan TJ (2012) Damage control for clay masonry infills in the design of RC frame structures. J Earthq Eng 16(sup1):1–35

Kakaletsis D (2009) Masonry infills with window openings and influence on reinforced concrete frame constructions. WIT Trans Built Environ 104:445–455
Kakaletsis D, Karayannis C (2007) Experimental investigation of infilled R/C frames with eccentric openings. Struct Eng Mech 26(3):231–250
Kakaletsis DJ, Karayannis CG (2008) Influence of masonry strength and openings on infilled R/C frames under cyclic loading. J Earthq Eng 12(2):197–221
Kakaletsis DJ, Karayannis CG (2009) Experimental investigation of infilled reinforced concrete frames with openings. ACI Struct J 106(2):132
Khoshnoud HR, Marsono K (2016) Experimental study of masonry infill reinforced concrete frames with and without corner openings. Struct Eng Mech 57(4):641–656
Kyriakides MA, Billington SL (2008) Seismic retrofit of masonry-infilled non-ductile reinforced concrete frames using sprayable ductile fiber-reinforced cementitious composites. In: The 14th world conference on earthquake Engineering, Beijing
Lowes L, Li J (2011) Background document FEMA P-58/BD/3.8. 6: fragility functions for reinforced concrete moment frames. Federal Emergency Management Agency, Washington, DC
Mansouri A, Marefat MS, Khanmohammadi M (2014) Experimental evaluation of seismic performance of low-shear strength masonry infills with openings in reinforced concrete frames with deficient seismic details. Struct Design Tall Spec Build 23(15):1190–1210
Mehrabi AB, Benson Shing P, Schuller MP, Noland JL (1996) Experimental evaluation of masonry-infilled RC frames. J Struct Eng 122(3):228–237. https://doi.org/10.1061/(ASCE)0733-9445(1996)122:3(228)
Misir IS, Ozcelik O, Girgin SC, Yucel U (2016) The behavior of infill walls in RC frames under combined bidirectional loading. J Earthq Eng 20(4):559–586
Morandi P, Hak S, Magenes G (2014). In-plane experimental response of strong masonry infills. In: 9th international masonry conference 2014, Guimaraes
Pereira MFP, Pereira MF, Ferreira JE, Lourenço PB (2011) Behavior of masonry infill panels in RC frames subjected to in plane and out of plane loads. In: 7th international conference on analytical models and new concepts in concrete and masonry structures
Petry S, Beyer K (2014) Influence of boundary conditions and size effect on the drift capacity of URM walls. Eng Struct 2014(65):76–88
Ricci P, De Risi MT, Verderame GM, Manfredi G (2013) Influence of infill distribution and design typology on seismic performance of low-and mid-rise RC buildings. Bull Earthq Eng 11(5):1585–1616
Ricci P, De Risi MT, Verderame GM, Manfredi G (2016) Procedures for calibration of linear models for damage limitation in design of masonry-infilled RC frames. Earthq Eng Struct Dyn 45(8):1315–1335
Ricci P, Di Domenico M, Verderame GM (2017) Experimental assessment of the out-of-plane seismic response of URM infill walls. In: ANIDIS 2017, Pistoia
Ross SM (2003) Peirce's criterion for the elimination of suspect experimental data. J Eng Technol 20(2):38–41
Saneinejad A, Hobbs B (1995) Inelastic design of infilled frames. J Struct Eng 121(4):634–650
Sassun K, Sullivan TJ, Morandi P, Cardone D (2016) Characterising the in-plane seismic performance of infill masonry. Bull N Z Soc Earthq Eng 49(1):100–117
Schwarz S, Hanaor A, Yankelevsky DZ (2015) Experimental response of reinforced concrete frames with AAC masonry infill walls to in-plane cyclic loading. In Structures, vol 3, pp 306–319
Sigmund V, Penava D (2012) Experimental study of masonry infilled R/C frames with opening. In: Proceedings of the 15WCEE, Lisbon
Stafford Smith B (1962) Lateral stiffness of infilled frames. ASCE J Struct Div 88(ST6):183–199
Stavridis A (2009) Analytical and experimental study of seismic performance of reinforced concrete frames infilled with masonry walls. University of California, San Diego
Suzuki T, Choi H, Sanada Y, Nakano Y, Matsukawa K, Paul D, Gulkan P, Binici B (2017) Experimental evaluation of the in-plane behaviour of masonry wall infilled RC frames. Bull Earthq Eng 15(10):4245–4267
Turgay T, Durmus MC, Binici B, Ozcebe G (2014) Evaluation of the predictive models for stiffness, strength, and deformation capacity of RC Frames with masonry infill walls. ASCE J Struct Eng 140(10):06014003
Velázquez-Dimas J, Quiñonez-Esquivel B, Castorena-González J, Reyes-Salazar A, González-Cuevas J, López-López D (2012) In-plane behaviour of confined masonry walls with holes retrofitted with GFRP and subjected to lateral cyclic loading. In: Proceedings of the 15th Word Conference of Earthquake Engineering, Lisbon, Portugal
Verderame G.M., Ricci P., Del Gaudio C. & De Risi M.T. (2016), Experimental tests on masonry infilled gravity- and seismic-load designed RC frames, Brick and Block Masonry: Trends, Innovations and Challenges - Proceedings of the 16th International Brick and Block Masonry Conference, IBMAC 2016, pp. 1349-1358

Waly (2010) Experimental and analytical work on the seismic performance of different types of masonry infilled reinforced concrete frames under cyclic loading, M.sc thesis, School of Natural and Applied Sciences of Dokuz Eylül University
Zarnic R, Tomazevic M (1984) The behaviour of masonry infilled reinforced concrete frames subjected to cyclic lateral loading. In: Proceedings of the 8th world conference on earthquake engineering, San Francisco, Prentice-Hall
Zhai C, Kong J, Wang X, Chen Z (2016) Experimental and finite element analytical investigation of seismic behavior of full-scale masonry infilled RC frames. J Earthquake Eng 20(7):1171–1198
Zovkic J, Sigmund V, Guljas I (2013) Cyclic testing of a single bay reinforced concrete frames with various types of masonry infill. Earthq Eng Struct Dyn 42:1131–1149

Affiliations

Carlo Del Gaudio[1] · Maria Teresa De Risi[1] · Paolo Ricci[1] · Gerardo Mario Verderame[1]

Carlo Del Gaudio
carlo.delgaudio@unina.it

Paolo Ricci
paolo.ricci@unina.it

Gerardo Mario Verderame
verderam@unina.it

[1] Department of Structures for Engineering and Architecture (DIST), University of Naples Federico II, Via Claudio 21, 80125 Naples, Italy